**Atmospheric
Chemistry
and Physics
Discussions**

Characterization of the sources and processes of organic and inorganic aerosols in New York City with a high-resolution time-of-flight aerosol mass spectrometer

Y.-L. Sun[1], Q. Zhang[1], J. J. Schwab[2], K. L. Demerjian[2], W.-N. Chen[3], M.-S. Bae[2,*], H.-M. Hung[4], O. Hogrefe[2], B. Frank[5], O. V. Rattigan[5], and Y.-C. Lin[3]

[1]Department of Environmental Toxicology, University of California, 1 Shields Ave., Davis, California 95616, USA
[2]Atmospheric Sciences Research Center, State University of New York at Albany, Albany, New York, USA
[3]Research Center for Environmental Changes, Academia Sinica, Taipei, Taiwan
[4]Department of Atmospheric Sciences, National Taiwan University, Taipei, Taiwan
[5]Division of Air Resources, New York State Department of Environmental Conservation, Albany, New York, USA
[*]now at: Environmental Engineering Department, Mokpo National University, South of Korea

ACPD

10, 22669–22723, 2010

Characterization of organic and inorganic aerosols in New York City

Y.-L. Sun et al.

Title Page

Abstract | Introduction

Conclusions | References

Tables | Figures

◄◄ | ►►

◄ | ►

Back | Close

Full Screen / Esc

Printer-friendly Version

Interactive Discussion

Characterization of organic and inorganic aerosols in New York City

Y.-L. Sun et al.

Title Page

Abstract	Introduction
Conclusions	References
Tables	Figures

|◄   ►|

◄   ►

Back   Close

Full Screen / Esc

Printer-friendly Version

Interactive Discussion

Abstract

Submicron aerosol particles (PM_1) were measured in-situ using a High-Resolution Time-of-Flight Aerosol Mass Spectrometer (HR-ToF-AMS) during the summer 2009 Field Intensive Study at Queens College in New York City. Organic aerosol (OA) and sulfate are the two dominant species, accounting for 54% and 24%, respectively, of total PM_1 mass on average. The average mass size distribution of OA presents a small mode peaking at ~150 nm (D_{va}) in addition to an accumulation mode (~550 nm) that is internally mixed with sulfate, nitrate, and ammonium. The diurnal cycles of sulfate and OA both show pronounced peaks between 01:00–02:00 p.m. EST due to photo-chemical production. The average ($\pm 1\sigma$) oxygen-to-carbon (O/C), hydrogen-to-carbon (H/C), and nitrogen-to-carbon (N/C) ratios of OA in NYC are 0.36($\pm$0.09), 1.49($\pm$0.08), and 0.012($\pm$0.005), respectively, corresponding to an average organic mass-to-carbon (OM/OC) ratio of 1.62($\pm$0.11). Positive matrix factorization (PMF) of the high resolution mass spectra identified five OA components: a hydrocarbon-like OA (HOA), two types of oxygenated OA (OOA) including a low-volatility OOA (LV-OOA) and a semi-volatile OOA (SV-OOA), a cooking-emission related OA (COA), and a unique nitrogen-enriched OA (NOA). HOA appears to represent primary OA (POA) from urban traffic emissions. It comprises primarily of reduced species (H/C=1.83; O/C=0.06) and shows a mass spectral pattern very similar to those of POA from fossil fuel combustion, and corre-lates tightly with traffic emission tracers including elemental carbon and NO_x. LV-OOA, which is highly oxidized (O/C=0.63) and correlates well with sulfate, appears to be representative for regional, aged secondary OA (SOA). SV-OOA, which is less oxi-dized (O/C=0.38) and correlates well with non-refractory chloride, likely represents less photo-chemically aged, semi-volatile SOA. COA shows a similar spectral pattern to the reference spectra of POA from cooking emissions and a distinct diurnal pattern peaking around local lunch and dinner times. In addition, NOA is characterized with prominent $C_xH_{2x+2}N^+$ peaks likely from amine compounds. Our results indicate that cooking-related activities are a major source of POA in NYC, releasing comparable

Full Screen / Esc

amounts of POA as traffic emissions. POA(=HOA+COA) on average accounts for ~30% of the total OA mass during this study while SOA dominates the OA composition with SV-OOA and LV-OOA on average accounting for 34% and 30%, respectively, of the total OA mass. The chemical evolution of SOA in NYC involves a continuous oxidation from SV-OOA to LV-OOA, which is further supported by a gradual increase of O/C ratio and a simultaneous decrease of H/C ratio in total OOA. Detailed analysis of NOA (5.8% of OA) presents evidence that nitrogen-containing organic species such as amines might have played an important role in the atmospheric processing of OA in NYC, likely involving acid-base chemistry. Analysis of air mass trajectories and satellite imagery of aerosol optical depth (AOD) indicates that the high potential source regions of secondary sulfate and aged OA are mainly located in regions to the west and southwest of the city.

1 Introduction

Aerosol particles play significant roles in climate change by altering the radiative balance of the Earth's atmosphere directly and indirectly (IPCC, 2007). They also constitute a threat to public health by increasing the risk of morbidity and mortality of sensitive groups (Pope et al., 2002, 2009). Fine particulate matter (PM) in densely populated megacity environments are of particular concern for their adverse effects on human health and regional air quality (Molina and Molina, 2004). The New York City (NYC) metropolitan area is one of the most populous megacities in the world and among the most polluted cities in the US by fine PM and ozone (American Lung Association's Report, 2010). Atmospheric aerosols are influenced by various emission sources and transformation processes. Characterizing the chemical composition and dynamic variations of aerosols in large urban environments such as NYC is important to unravel the complexities of anthropogenic aerosols and supporting health outcome studies (Demerjian and Mohnen, 2008; Wexler and Johnston, 2008).

A number of studies conducted in recent years characterized inorganic species (e.g., sulfate, nitrate, and ammonium), carbonaceous material (e.g., organic and elemental carbon; OC and EC), and trace metal species in aerosols in metropolitan NY (Schwab et al., 2004; Bae et al., 2006; Dutkiewicz et al., 2006; Qin et al., 2006; Venkatachari et al., 2006; Sunder Raman et al., 2008; Rattigan et al., 2010). Sulfate and OC usually dominate fine PM composition in the region. While sulfate is mainly contributed by regional transport, organic aerosol (OA) have contributions from both local and regional accumulation (Dutkiewicz et al., 2004; Lall and Thurston, 2006; Qin et al., 2006). Particulate organic materials can be classified as either primary OA (POA) from direct emissions, e.g., fossil fuel and biomass burning, or secondary OA (SOA) from the oxidation of gas-phase precursors (Kanakidou et al., 2005). SOA has been identified as a major contributor to the fine PM burden in NYC, especially under summertime conditions. Using the EC tracer method, Rattigan et al. (2010) estimated that SOA accounted for 63–73% and 40–50% of total OC during summer and winter, respectively, in South Bronx, NY. In addition, by analyzing ambient aerosol data acquired with an Aerodyne Aerosol Mass Spectrometer (AMS, Canagaratna et al., 2007), Zhang et al. (2007a) reported that oxygenated OA (OOA), a surrogate for SOA, on average accounted for 70% and 50% of total OA mass in Queens, NY during summer and winter, respectively.

Two AMS studies were conducted in summer 2001 (Drewnick et al., 2004a,b) and winter 2004 (Weimer et al., 2006), respectively, on the campus of Queens College (QC) in NYC as part of the $PM_{2.5}$ Technology Assessment and Characterization Study-NY (PMTACS-NY) – one of the EPA supersite programs (Demerjian and Mohnen, 2008). These real-time, highly time-resolved measurements of the concentrations and size distributions of non-refractory submicron aerosol ($NR-PM_1$) species (i.e., organics, sulfate, nitrate, ammonium, and chloride) offered valuable insights into the chemistry, sources, and evolution processes of fine PM in NYC (Drewnick et al., 2004a,b; Weimer et al., 2006; Demerjian and Mohnen, 2008; Wexler and Johnston, 2008). An interesting observation was a distinct small particle mode (~70 nm) of organics in summer

that was externally mixed with sulfate and nitrate (Drewnick et al., 2004b). This mode appeared to be related to traffic emissions as it intensified during morning rush-hour (Drewnick et al., 2004a). In addition, significant differences in aerosol composition and size distributions were observed in winter at the same site due to different meteorolog-
5 ical conditions and photochemical processing (Weimer et al., 2006).

The AMS used during PMTACS-NY 2001 and 2004 was equipped with a Quadrupole mass spectrometer (i.e., Q-AMS; Jayne et al., 2000) which generated unit mass resolution (UMR) spectra. In summer 2009 we returned to the same site with a new advanced version of the AMS – a High-Resolution Time-of-Flight AMS (HR-ToF-AMS,
10 termed as HR-AMS hereafter) (DeCarlo et al., 2006). Compared to the Q-AMS, the HR-AMS is significantly improved on chemical resolution and sensitivity, especially allows us to study in greater detail the chemical composition and atmospheric processing of OA. Here we report the main findings from this study, including (1) evaluation of HR-AMS based on the comparisons of measurements with collocated instruments;
15 (2) mass concentrations, size distributions, chemical composition, and temporal and diurnal variations of PM_1 species; (3) elemental composition of OA; (4) determination of OA components via Positive Matrix Factorization (PMF) of the high-resolution mass spectra (HRMS); and (5) investigation of the sources and processes of organic and inorganic aerosol components.

20 ## 2   Methods

2.1   Sampling site and instrumentation

This study took place from 13 July through 3 August 2009 on the campus of Queens College (40.74° N, 73.82° W, ~25 m a.s.l.; Fig. S1 in the supplementary information). The HR-AMS measurements were conducted inside the state-of-the-art Atmospheric
25 Sciences Research Center-Mobile Laboratory (ASRC-ML) (Schwab et al., 2010) along with various fast-response aerosol and gas instruments. These instruments include

a DMT single-wavelength Photoacoustic Soot Spectrometer (PASS-1), a TSI Fast Mobility Particle Sizer (FMPS, Model 3091, 5.6–560 nm) spectrometer, a TSI water Condensation Particle Counter (CPC, Model 3781), an Aerodyne Quantum Cascade Laser (QCL) Spectrometer for measurements of formaldehyde and NO_2, a Li-COR CO_2 an-
5 alyzer, a BTEX analyzer for benzene, toluene, ethylbenzene, and xylenes, and 2B technologies analyzers for O_3, NO, and NO_2. The ASRC-ML was parked at Lot 6 (Site B in Fig. S1) during this study except for two mornings on 28 and 30 July, and two evenings on 27 July and 1 August when it was moved to Lot 15 (Site C in Fig. S1) to measure near-road traffic plumes. Lot 6 is located approximately 500 m south to
10 the Long Island Expressway (LIE, I-495) and 1.2 km east to the Van Wyck Expressway (I-678), two high-traffic highways in the NYC metropolitan area. Lot 15 is on the immediate south side of I-495, ∼500 m to the northeast of Lot 6. During part of this study, an Aerodyne Mobile Laboratory was also deployed, in which a novel Soot Particle-AMS (SP-AMS) was operated alongside a number of aerosol and gas instruments.
15 In addition to measurements from the mobile facilities, aerosol and gas species were also measured inside a one-story building complex (Site A in Fig. S1) situated at ∼140 m north of Lot 6. This was the same sampling site for the PMTACS-NY 2001 summer and 2004 winter campaigns. Detailed descriptions of this site are given in Drewnick et al. (2004a) and Weimer et al. (2006). A key instrument deployed at Site
20 A is a Particle-into-Liquid Sampler (PILS) coupled with two Metrohm Compact 761 Ion Chromatography (IC) systems (Herisau, Switzerland). The IC systems were equipped with an A Supp 5-250 and a C 4 column, respectively, for simultaneous measurements of anions and cations every 30 min. Ambient air was sampled into the PILS, in sequence, after a URG $PM_{2.5}$ cyclone, a VOC denuder, and two URG 2000 annular glass
25 denuders coated with sodium carbonate and citric acid to remove acidic and basic gases, respectively. The IC systems were calibrated every 3–5 days, and the denuders were regenerated every week. In order to account for volatile losses, a correction factor of 1.14 (=1/0.88) suggested by Sorooshian et al. (2006) was applied for ammonium quantification.

In addition to the PILS-IC, other aerosol instruments deployed in the building complex include a Sunset Lab OC/EC Analyzer, a long- and a nano- Scanning Mobility Particle Sizer (SMPS), a Thermo Electron 5020 Sulfate Particulate Analyzer (SPA), a Tapered Element Oscillating Microbalance (TEOM), and an Aerodyne Aerosol Chemical Speciation Monitor (ACSM).

All the data in this study are reported at ambient temperature and pressure (∼101 kPa) conditions in Eastern Standard Time (EST), which equals Coordinated Universal Time (UTC) minus 5 h or Local Time (i.e., Eastern Daylight Time - EDT) minus 1 h.

2.2 HR-AMS operation

Ambient air was sampled isokinetically into the HR-AMS from a 1.0 inch O.D. stainless steel tube with an inline $PM_{2.5}$ cyclone (URG-2000-30EH). The inlet of sampling line was positioned on the top of ASRC-ML at ∼2 m above the ground. The residence time of air between the inlet and the HR-AMS was estimated at ∼5 s. The HR-AMS was operated under the "V" and "W" ion optical modes alternatively every 5 min. The V-mode is more sensitive while the W-mode has higher mass resolution. Under V-mode operation, the AMS cycled through the mass spectrum (MS) mode and the particle time-of-flight (PToF) mode every 30 s, spending 10 s and 20 s, respectively, in each mode. Size distribution data are reported in units of mass-weighted aerodynamic diameter. No PToF data were sampled in W-mode due to limited signal-to-noise (S/N) ratio. However, the high mass resolution (∼5000–6000) of W-mode allows us to determine the ion-specific mass spectra and thus the elemental compositions of OA (DeCarlo et al., 2006; Aiken et al., 2008). The HR-AMS was calibrated for ionization efficiency (IE) and particle sizing at the beginning and in the middle of this study following the standard protocols (Jayne et al., 2000; Jimenez et al., 2003; Drewnick et al., 2005). The detection limits (DLs) of NR-PM$_1$ species were determined as 3 times the standard deviations (3σ) of the corresponding signals in particle-free ambient air through a HEPA filter (Zhang et al., 2005b). The 5-min DLs of organics, sulfate, nitrate, ammonium,

and chloride are 57, 5, 4, 23, and 5 ng/m^3, respectively for V-mode and 110, 24, 30, 151, and 22 ng/m^3, respectively for W-mode, which are close to the values reported in previous studies (DeCarlo et al., 2006; Sun et al., 2009).

2.3 HR-AMS data analysis

2.3.1 General analysis

The mass concentrations and size distributions of NR-PM$_1$ species were analyzed using the standard AMS data analysis software (SQUIRREL v1.46, Sueper, 2010) written in Igor Pro (Wavemetrics, Lake Oswego, OR). A collection efficiency (CE) of 0.5 was introduced to account for the incomplete detection of aerosol species due to particle bounce at the vaporizer and/or partial transmission of particles by the lens (Huffman et al., 2005). The value of 0.5 was validated based on inter-comparisons with collocated measurements (see Sect. 3.1) and is consistent with the observed aerosol composition and the CE values observed in previous AMS campaigns at the same site (Drewnick et al., 2004a; Weimer et al., 2006). Relative ionization efficiencies (RIEs) of 1.4 for organics, 1.2 for sulfate, 1.1 for nitrate, and 1.3 for chloride were used as previously reported (Allan et al., 2003b; Jimenez et al., 2003). The RIE for ammonium was determined at 4.0 based on the analysis of pure NH_4NO_3 particles during this study.

2.3.2 High resolution mass spectra analysis

The HRMS of both V- and W-mode were analyzed using the PIKA – software toolkit downloaded at http://cires.colorado.edu/jimenez-group/ToFAMSResources/ ToFSoftware/index.html. The W-mode spectra were analyzed to determine the elemental compositions of ion fragments, and subsequently the hydrogen-to-carbon (H/C), oxygen-to-carbon (O/C), nitrogen-to-carbon (N/C), and organic mass-to-carbon (OM/OC) ratios of OA (Aiken et al., 2008). Since the organic H_2O^+, HO^+, O^+, and CO^+ signals were not measured directly due to large uncertainties, they were scaled

Characterization of organic and inorganic aerosols in New York City

Y.-L. Sun et al.

according to the organic CO_2^+ signal using the ratios suggested by Aiken et al. (2008), i.e., $CO^+=CO_2^+$, $H_2O^+=0.225CO_2^+$, $HO^+=0.25H_2O^+$ and $O^+=0.04H_2O^+$. Additionally, elemental analysis was also performed to the V-mode spectra using the same ion fragments identified for the W-mode spectra. Very similar O/C, H/C, and OM/OC ratios as those from W-mode were observed. However, the V-mode N/C ratios are on average a factor of 2 different from the W-mode results, due to larger uncertainties in quantifying $C_xH_yN_p^+$ ions using the lower resolution V-mode spectra.

2.3.3 PMF analysis of high resolution mass spectra

PMF analysis (Paatero and Tapper, 1994) was performed to the HRMS, i.e., the ion-speciated W-mode spectra, using the PMF Evaluation Toolkit (PET) v2.02 (Ulbrich et al., 2009). The error matrix for PMF analysis is determined based on propagation of errors of Poisson counting statistics and electronic noise (DeCarlo et al., 2010). The peak fitting errors calculated from the residuals of PIKA fitting were also considered for small ions situated in close proximity to large ions. Ions with S/N ratio <0.2 (Paatero and Hopke, 2003) were removed from the HRMS data and error matrices before PMF analysis. Excluding these noisy ions improves the differentiation of OA components, but has little impact on the mass concentrations since they together account for only ~2% of total OA signal. The "weak" ions with S/N between 0.2 and 2 were downweighed by increasing their errors by a factor of 2 (Paatero and Hopke, 2003; Ulbrich et al., 2009). In addition, H_2O^+, HO^+, O^+, and CO^+ were removed from the data and error matrices before PMF analysis because they were determined according to the relationship with CO_2^+; including of which may introduce additional weight to CO_2^+ (Ulbrich et al., 2009). They were inserted back into the mass spectral matrix after PMF analysis.

A summary of the PMF results is presented in Fig. S2. After an extensive evaluation of the mass spectral profiles and time series of different number of factors and the rotational forcing parameter fPeak, the 5-factor solution with fPeak=0($Q/Q_{expected}$=3.6) was chosen. The OA components of the 5-factor solution solved under different fPeak

values show very similar mass spectral patterns and time series (Fig. S2). The direct comparisons of the mass spectra and time series of 4-factor and 6-factor solution are shown in Fig. S3. The 4-factor solution does not resolve the small, yet distinct, fifth factor (~6% of total OA) (see Sect. 3.5.4 for details). The 6-factor solution, however, shows evidence of unrealistic "split" of the semi-volatile OOA (SV-OOA) factor. A detailed list of reasons for the selection of 5 factors is given in Table S1.

2.4 Air mass trajectories and aerosol optical depth

3-day back trajectories arriving at QC were calculated every 1 h over the time period of this study using the National Oceanic and Atmospheric Administration (NOAA) HYS-PLIT 4.8 model (Draxler and Rolph, 2003) and the meteorological input from Air Resources Laboratory FNL data archive. 490 trajectories in total were obtained. These trajectories were then categorized into four clusters, i.e., cluster 1 from northwest (7.3% of time), cluster 2 from west (37.3% of time), cluster 3 from the Atlantic Ocean (24.5% of time), and cluster 4 from southwest (30.8% of time), using the trajectory cluster analysis of the HYSPLIT 4.8 model.

Aerosol optical depth (AOD) was retrieved from the observations at wavelength of 550 nm made by National Aeronautics and Space Administration (NASA) Moderate Resolution Imaging Spectroradiometer (MODIS) onboard the Terra satellite. The Collection 5 level 2 data was used in this study (http://ladsweb.nascom.nasa.gov/browse_images/l2_browser.html?form=AADS&browseType=Level+2). The algorithm of retrieval and validation of retrieved AOD is described in detail in Remer et al. (2005).

3 Results and discussions

3.1 Inter-comparisons

Figure 1 shows the inter-comparisons of measurements by the HR-AMS and other collocated instruments. Overall, the HR-AMS results correlate well with those of

TEOM, PILS-IC, SPA, and Sunset Lab OC/EC Analyzer (r^2=0.47–0.90). NR-PM$_1$ in total (=sulfate+nitrate+organics+ammonium+chloride) reports 68% of the TEOM PM$_{2.5}$ mass, mainly because the HR-AMS only detects PM$_1$ and does not respond to refractory components such as black carbon and crustal materials. An intercept of

5   3.91 µg/m^3 for the linear regression of AMS total vs. TEOM mass is likely due to the losses of semi-volatile materials at 50 °C inside TEOM (Eatough et al., 2003). The AMS sulfate, nitrate, and ammonium account for ∼71–76% of those in PM$_{2.5}$ from PILS-IC measurements. These comparisons are consistent with previous observations at other urban sites, e.g., Pittsburg (Zhang et al., 2005b),Tokyo, Japan (Takegawa et al., 2005),

10 and Mexico City (Salcedo et al., 2006). Note that during PMTACS-NY 2001 and 2004 the correlations between Q-AMS and PILS-IC measurements were close to 1:1 for both sulfate and nitrate (Drewnick et al., 2003, 2004a; Weimer et al., 2006). However, a CE value of 0.43 was applied in previous studies comparing to CE=0.5 used in this analysis.

15   While the chloride concentrations measured by the HR-AMS correlate with those by the PILS-IC (r^2=0.47, Fig. 1f′), the HR-AMS on average reports only ∼35% of the chloride measured by PILS. In addition, there are times when the AMS-chloride is much lower than the PILS-chloride (e.g., 09:00 a.m.–20:00 p.m., 31 July, Fig. 1f). This is probably because the HR-AMS measures primarily NR-chloride (e.g., in the form of

20 NH$_4$Cl) and is insensitive to refractory species such as NaCl and KCl at its vaporizer temperature of 600 °C. Indeed, significantly elevated signals of chloride (e.g., ^{35}Cl$^+$ and ^{37}Cl$^+$) are observed in the "closed" (or "background") mass spectra acquired during this study, indicating the detection of considerable amounts of refractory-chloride. Refractory species, such as lead, evaporate slowly, yet continuously, on the AMS oven and

25 thus show elevated signals in the "background" spectra (Salcedo et al., 2010). Given the proximity of NYC to the Atlantic Ocean, significant amounts of refractory-chloride are likely present in airborne PM$_1$.

     Although the HR-AMS organic concentrations show tight correlation with the OC concentrations measured by a Sunset Lab OC/EC Analyzer (r^2=0.79), the linear

regression slope of 2.59 is higher than the average OM/OC ratio of 1.62 determined via elemental analysis of the HRMS (Sect. 3.3). The typical OM/OC ratios observed at urban sites range ∼1.6–1.8 (Turpin and Lim, 2001; Takegawa et al., 2005; Zhang et al., 2005b; Bae et al., 2006; Aiken et al., 2008). Note that Weimer et al. (2006) also observed relatively high slopes of 2.06–2.72 in winter 2004 at QC comparing Q-AMS vs. Sunset OC measurements. Possible reason for this could be: 1) evaporative losses of semi-volatile species during the carbon analysis, which is consistent with the observation that semi-volatile organic species compose a large fraction of OA in NYC (see Sect. 3.5.1), and 2) "over-correction" of the OC data using the blank filter values (Bae et al., 2006).

3.2 Mass concentration, composition, and diurnal variation of submicron aerosol particles

Figure 2 shows the time variations of total PM_1 mass, the mass fractional contributions of individual species, and the meteorological conditions during the entire campaign. The PM_1 concentration and composition vary dynamically with high aerosol loadings generally associated with southerly wind. Low PM_1 loading periods typically occur with northwesterly wind. The total mass concentrations of PM_1 (including EC) vary between 2.08 and 35.8 $\mu g/m^3$ during this study. Organics frequently comprise the largest fraction of PM_1 with sulfate being the second largest (Fig. 2d). On average, organics and sulfate account for 54.3% (24.5–96.5%) and 24.2% (0.7–54.8%), respectively, of PM_1 mass (Table 1). The dominance of organics and sulfate is similar to previous observations at the same site in summer 2001 (Drewnick et al., 2004a). The average loading of PM_1 is also similar between this study (11.7 $\mu g/m^3$) and summer 2001 (12.5 $\mu g/m^3$) (Drewnick et al., 2004a; Weimer et al., 2006). However, on average sulfate is lower by ∼31% and organics higher by ∼9% in 2009 compared to 2001. The decrease in sulfate is likely the results of reduction in SO_2 emission in NYC (e.g., by more than a factor of 2 in 2009 compared to 2001; http://www.dec.ny.gov/chemical/54358.html), part of which is probably due to the introduction of ultra low sulfur diesel fuel starting in 2006,

although differences in wind patterns between the 2001 and 2009 study periods might have also played a role.

While nitrate overall represents a minor fraction of PM_1 (4.2%), high fraction of nitrate (up to 30–40% of PM_1) are observed during some time periods (e.g., 02:00–04:00 a.m., 22 July, Fig. 2). The average EC concentration of 0.70 μg/m^3 (6% of PM_1) is close to the values observed in NYC previously, e.g., 0.75±0.20 μg/m^3 from 2002–2004 at QC (Bae et al., 2006) and 0.5–1.4 μg/m^3 from 2006–2008 at South Bronx (Rattigan et al., 2010), but 2–4 times higher than those at rural sites in NY, e.g., 0.18±0.20 μg/m^3 at Pinnacle State Park (Bae et al., 2006) and 0.31 and 0.36 μg/m^3, respectively, at Potsdam and Stockton (Sunder Raman et al., 2008). Note that the EC in this paper refers to optically measured EC with higher time resolution (1-min), but it shows good agreement with thermal measurement of EC (r^2=0.86, slope=0.93). A weekday vs. weekend comparison of the concentrations of NR-PM_1 species shows almost no difference for sulfate (1.5%) and ∼8–28% lower concentration for the other NR species during weekend. EC shows the largest decrease in concentration (on average 35%) during weekend, similar to observations made in South Bronx (Rattigan et al., 2010).

The average diurnal cycles of aerosol species are shown in Fig. 3. Organics show a small early morning peak between 05:00–06:00 a.m. (i.e., 06:00–07:00 a.m. LT) and a distinct early afternoon peak between 12:00–14:00 p.m. The morning peak correlates with that of EC, which is primarily due to local traffic emissions. The early afternoon peak of organics is mostly contributed by oxygenated species as the result of photochemical formation of SOA and by emissions of POA from cooking-related activities as well (Sect. 3.5.3). The high concentration of organics at night is likely due to increased traffic from heavy duty diesel trucks (to avoid commuter traffic; Venkatachari et al., 2006) compounded with less dilution due to shallow boundary layer. Indeed, substantially elevated EC (Fig. 3a) and HOA (Sect. 3.5.2) are clearly seen at night.

Sulfate shows an early afternoon peak at ∼13:00–14:00 p.m., similar to that observed in summer 2001 (Drewnick et al., 2004a). In order to investigate the source of this peak, the diurnal production rate of sulfuric acid was estimated based on gas phase

bi-molecule association reaction of $SO_2 + \bullet OH + M \rightarrow HOSO_2 + M$. The $\bullet OH$ concentration data used for the calculation was acquired in the same month during PMTACS-NY 2001 at the same location (Ren et al., 2003). The calculation formula is presented in Appendix A and the diurnal profile of the production rate of sulfuric acid is shown in Fig. 4a, in which gaseous CO_2 is used as an indicator of dilution effects associated with changes in boundary layer height. The gas phase production rate of sulfuric acid peaks at early afternoon together with sulfate, counteracting the dilution associated with higher boundary layer that clearly leads to a gradual drop in the concentrations of primary emission species (e.g., CO_2, NO_x, EC, and HOA) during daytime. However given the slow gas phase production rate of H_2SO_4, which leads to an integrated production of $\sim 0.35\,\mu g/m^3$ of sulfate between 08:00 a.m. to 14:00 p.m. compared to an observed increase of $\sim 1\,\mu g/m^3$ (Fig. 4a), local photochemical transformation of SO_2 to sulfate via gas-phase oxidation is inadequate to account for the observed sulfate production. Regional transport and/or aqueous processes may have played a significant role. The relatively flat diurnal pattern and a general trend of multi-day build-up signify the regional influences on sulfate in NYC, consistent with the regional character of sulfate in the Northeastern US (Dutkiewicz et al., 2004; Zhang et al., 2005b; Qin et al., 2006).

Both nitrate and chloride show similar diurnal cycles with the highest concentration appearing in early morning (04:00–07:00 a.m., Fig. 3d,f). The diurnal cycle of nitrate is mainly driven by HNO_3 production, gas-to-particle partitioning to form ammonium nitrate, and boundary layer dynamics (Zhang et al., 2005b; Salcedo et al., 2006). The production rate of HNO_3 was estimated from the reaction of $NO_2 + \bullet OH + M \rightarrow HONO_2 + M$, which is the main formation mechanism of nitrate during daytime (Appendix A). The gas-to-particle partitioning of NH_4NO_3 is strongly temperature and RH dependent, and the diurnal variation of the equilibrium constant (K_p) of $NH_3(g) + HNO_3(g) \leftrightarrow NH_4NO_3(s)$ is shown in Fig. 4b (see Appendix A for calculations). Note that the formation of $NH_4NO_3(s)$ is also controlled by the acidity of particles – acidic particles retain very little nitrate (Zhang et al., 2007b). However, PM_1 appears to

Characterization of organic and inorganic aerosols in New York City

Y.-L. Sun et al.

Title Page

Abstract	Introduction
Conclusions	References
Tables	Figures

|◄ | ►|

◄ | ►

Back | Close

Full Screen / Esc

Printer-friendly Version

Interactive Discussion

be bulk neutralized for a large fraction of time during this study (Sect. 3.5.4). Despite intense daytime production of HNO_3 (at peak rate of 5.6 µg m^{-3} h^{-1}, Fig. 4b), the diurnal cycle of nitrate shows overall similar variation pattern as those of K_p and CO_2q, which decrease during daytime and reach minimum at ∼02:00 p.m. EST. These results suggest that gas-to-particle partitioning of HNO_3 controls the diurnal variation of nitrate in NYC. Similar diurnal pattern of nitrate was observed in Pittsburgh (Zhang et al., 2005b) and at the same site in summer 2001 (Drewnick et al., 2004a). However, significantly different patterns were observed in both Mexico City (Salcedo et al., 2006; Aiken et al., 2009) and Beijing in 2006 (Sun et al., 2010), where daytime photochemical production of HNO_3 is much faster likely due to considerably higher NO_x emissions. The diurnal cycle of ammonium is very similar to the sum of sulfate and nitrate as ammonium presents mainly in the form of ammonium sulfate and ammonium nitrate.

3.3 Bulk composition and elemental ratios of OA

Figure 5a,b show the average HRMS of OA colored by the contributions of elements and ion categories, respectively. The m/z 44 peak, mainly contributed by CO_2^+ (92%, Fig. 5c), is the base peak in the spectrum. m/z 57 (∼2% of OA), which has been suggested as an AMS spectral tracer for HOA (Zhang et al., 2005a), is also a significant peak. However, on average only 70% of signal at m/z 57 is the hydrocarbon ion – $C_4H_9^+$ (∼70%) and the rest 30% is an oxygenated ion $C_3H_5O^+$ (Fig. 5c). The bulk mass-based composition of OA in NYC is dominated by carbon (62.1%) and oxygen (29.3%) with a minor contribution from hydrogen (7.7%) and nitrogen (0.8%). The diurnal variations of elements all show a pronounced peak at 01:00 p.m. due to photochemical production despite deeper boundary layer (Fig. S4). A small morning peak of C, H, and N occurs between ∼05:00–06:00 a.m. due to local traffic emissions and a shallow boundary layer, consistent with that of EC. In contrast, the average mass fractions of elements show relatively flat diurnal patterns except slightly higher contributions of C in the morning and O during the afternoon (Fig. 5d). On a daily basis, the O/C ratio of OA_1 varies between 0.31–0.40 and OM/OC between 1.56–1.67 (Fig. 5e).

The average (±1σ) OM/OC ratio for the entire study is 1.62 (±0.11), which is consistent with the value of 1.6 (±0.2) suggested for urban aerosols (Turpin and Lim, 2001). The OM/OC ratios determined from a multi-year study at QC by comparing the reconstructed PM$_{2.5}$ mass and OC vary between 1.27 and 2.01 (Bae et al., 2006). The O/C ratio (0.36±0.09) of this study is also consistent with AMS observations at other urban sites, e.g., Mexico City (Aiken et al., 2008), Tokyo (Takegawa et al., 2005), and London (Allan et al., 2010). The OM/OC and O/C ratios both increase gradually from the morning to the late afternoon due to enhanced photochemical SOA formation (Fig. 5e). The H/C ratio (1.49±0.08) shows an opposite diurnal pattern with a significant morning peak due to local traffic influence. While the average N/C ratio of 0.012 (±0.004) is similar to the values observed from previous HR-AMS studies (DeCarlo et al., 2008; Aiken et al., 2009; Sun et al., 2009), periods with much higher N/C ratio (~0.03–0.04) are also observed, likely due to the formation of N-containing organic compounds (Sect. 3.5.4).

3.4 Chemically-resolved size distributions of submicron aerosol particles

The average size distribution of aerosol species and the size-resolved aerosol composition for the entire campaign are shown in Fig. 6. We derived the size distribution of EC based on m/z 57 after removing the contribution of $C_3H_5O^+$ (Fig. 7), assuming the distribution pattern of EC mirrors that of $C_4H_9^+$ – a dominant hydrocarbon ion at m/z 57 (Fig. 5c). The rationales behind this assumption are: 1) $C_4H_9^+$ (or m/z 57 of the unit resolution AMS data) is an AMS spectral tracer for HOA (Canagaratna et al., 2004; Zhang et al., 2005a; Aiken et al., 2008), and 2) HOA is a surrogate for combustion-related POA in urban areas (Zhang et al., 2005c, 2007a; Jimenez et al., 2009; Ulbrich et al., 2009; Allan et al., 2010; Ng et al., 2010). Indeed, $C_4H_9^+$ correlates well with EC (r^2=0.42) and NO$_x$ (r^2=0.61). The assumption is also supported by the similar size distributions between m/z 57 and BC from the SP-AMS measurements of exhaust plumes of high duty trucks and Metropolitan Transportation Authority (MTA) standard buses during this campaign (Massoli et al., 2010). However, since $C_3H_5O^+$ contributes ~30% of the m/z 57 signal during this study, the size distribution of m/z 57 may be

influenced by oxygenated species that are secondary in origin. The fact that $C_3H_5O^+$ correlates poorly with $C_4H_9^+$ ($r^2=0.14$) indicate differences in their sources.

We estimated the size distribution of $C_3H_5O^+$ according to that of m/z 44, which is an AMS spectral tracer for OOA (Zhang et al., 2005a). $C_3H_5O^+$ correlates well with m/z 44 ($r^2=0.73$) and moderately with sulfate ($r^2=0.29$), a well-known secondary inorganic aerosol species. The size distributions of m/z 44 and sulfate also closely resemble each other (Figs. 7 and 3c). Note that upon these treatments, the accumulation mode of EC may nevertheless have been overestimated because of the contribution of OOA to $C_4H_9^+$ (~10% of the total $C_4H_9^+$ signals on average), especially in late afternoon when SOA production is intense. A support for this possibility is the better correlation of $C_4H_9^+$ with EC ($r^2=0.60$) and NO_x ($r^2=0.76$) during morning rush hours (04:00–08:00 a.m. EST) than other periods.

All aerosol species show an overlapping accumulation mode peaking at ~550 nm in vacuum aerodynamic diameter (D_{va}) (Fig. 6a). This mode dominates the size distributions of secondary aerosol species, i.e., sulfate, nitrate and ammonium, and m/z 44 as well. In addition, it usually persists throughout the day with relatively little variations in intensity (Fig. 3). However, a mode peaking at 100–150 nm shows up in the size distributions of organics, EC (Fig. 6), and m/z 57 (Fig. 7b), suggesting that primary carbonaceous particles are externally mixed with secondary species. Similar phenomena were observed at various other urban sites (Allan et al., 2003a; Alfarra et al., 2004; Drewnick et al., 2004b; Zhang et al., 2005b; Takegawa et al., 2006; Weimer et al., 2006; Huang et al., 2010; Sun et al., 2010).

During this study, ultrafine particles (<100 nm) are almost completely composed of carbonaceous material with EC contributing 24% of total mass and OA contributing an average 73%. EC is only a minor fraction (<5%) above 200 nm. The accumulation mode aerosols are mainly composed of organics and sulfate, which together account for ~80% of the total mass.

3.5 Determination of OA components and characterization of their sources and processes

PMF analysis of the HRMS of OA identified five OA components, of which the ion-speciated mass spectra and time series are shown in Fig. 8. These 5 components demonstrate distinct temporary variation and mass spectral patterns that are indicative of their association with unique sources and processes. In brief, 5 OA components include: 1) a highly oxidized and low-volatility OOA (LV-OOA; O/C=0.63), 2) a less ox-idized and semi-volatile OOA (SV-OOA; O/C=0.38), 3) a nitrogen-enriched OA (NOA) with a much higher N/C ratio (0.052) than other OA components (∼0.004–0.011), 4) a cooking-emission related OA (COA) which shows spectral features similar to those of POA from cooking emissions and a unique diurnal pattern peaking during lunch and dinner times, and 5) a hydrocarbon-like OA component (HOA) that represents POA from incomplete fossil fuel combustion given its low O/C ratio (0.06) and good cor-relation with combustion emission tracers such as NO_x and EC. Detailed discussions on each component, including the mass spectral profiles, correlations with the tracer species, temporal variation patterns, and associations with different sources and pro-cesses, are given in the following subsections.

3.5.1 Semi-volatile and low-volatility OOA (SV-OOA and LV-OOA)

The mass spectrum of LV-OOA (Fig. 8a) is characterized by a dominant peak at *m/z* 44 (CO_2^+), similar to the more oxidized OOA-1 component determined at other urban sites (Lanz et al., 2007; Ulbrich et al., 2009; Sun et al., 2010). Its O/C and OM/OC ratios (0.63 and 1.98, respectively) are in the range of the values of LV-OOA and total OOA (when LV- and SV-OOA are not separated) observed worldwide (Jimenez et al., 2009; Ng et al., 2010). The mass spectrum of SV-OOA (Fig. 8b), which has lower O/C ratio (0.38) and higher fraction of *m/z* 43 (f_{43}=9.3%, mainly $C_2H_3O^+$) compared to LV-OOA, also tracks the spectral pattern of previous-reported SV-OOA (Morgan et al., 2010; Ng et al., 2010).

A survey of the correlations between the five OA components and individual ions in the HRMS that are categorized into four ion families, i.e., $C_xH_y^+$, $C_xH_yO_1^+$, $C_xH_yO_2^+$, and $C_xH_yN_p^+$ ($x \geq 1$, $y \geq 0$, and $p \geq 1$) is shown in Fig. 9. LV-OOA shows most significant correlation with oxygenated ions containing two O atoms ($C_xH_yO_2^+$) followed by $C_xH_yO_1^+$, and very weak correlation with $C_xH_y^+$ and $C_xH_yN_p^+$. On average LV-OOA accounts for 51% and 38% of $C_xH_yO_2^+$ and $C_xH_yO_1^+$, respectively, for the entire study (Fig. 10). Apportionment of the ions of six major m/z's (Fig. 11) further reveals that that LV-OOA accounts for 53% of CO_2^+ (m/z 44), 61% of $C_2H_2O_2^+$ (m/z 58), and 46% of $C_2H_4O_2^+$ (m/z 60). Compared to LV-OOA, SV-OOA shows even tighter correlations with $C_xH_yO_1^+$ and slightly less, yet still high, correlations with $C_xH_yO_2^+$. It also correlates much better with $C_xH_y^+$ ions than LV-OOA does. On average, SV-OOA contributes 42% of the $C_xH_yO_1^+$ signal and 31% of the $C_xH_yO_2^+$ (Fig. 10). These results clearly indicate that the chemical compositions of the two OOA types are significantly different: SV-OOA comprises less oxygenated, possibly freshly oxidized species, while LV-OOA comprises highly oxidized species including di- and poly-carboxylic acids.

LV-OOA correlates well with sulfate (r^2=0.66, Fig. 8a and Table 2), consistent with previous studies at various sites showing that these two species are secondary in nature and mostly driven by regional production (Zhang et al., 2005c; Kondo et al., 2006; Volkamer et al., 2006). SV-OOA in general correlates with chloride and nitrate (Fig. 8b), indicating its semi-volatile characteristics (Ulbrich et al., 2009). The correlation between SV-OOA and chloride (r^2=0.30, Table 2) is stronger than that between SV-OOA and nitrate (r^2=0.05), mainly due to the occurrence of several nighttime nitrate plumes (e.g., 22 July). For instance, upon excluding the nitrate plume on 22 July (5% of total data points), the correlation between SV-OOA and nitrate improves to r^2=0.17. Nevertheless, total OOA(=LV-OOA+SV-OOA) correlates well with total secondary inorganic species (=sulfate+nitrate+chloride, r^2=0.50, Fig. 12a), marking the link between OOA and SOA. The ratio of total OOA/sulfate in NYC is 1.29 (Table 2), much higher than 0.38 observed in Pittsburgh (Zhang et al., 2005c), highlighting the importance of SOA

contribution to fine PM loading in NYC. Total OOA does not show much correlation with O_x (r^2=0.08), similar to the observations in Pittsburgh as well (Zhang et al., 2005c).

LV-OOA accounts for 30.3% of the OA mass on average, with the average contribution up to 46% during late afternoon and down to 22% at night (Fig. 13). SV-OOA accounts for an average 33.7% of the OA mass, showing a major contribution (~50%) in early morning. LV-OOA and SV-OOA together account for 64% of OA on average, similar to the estimated SOA contribution (63–73%) in NYC using the EC tracer method (Rattigan et al., 2010). In addition, OOA in total accounts for 81% of the O mass, 58% of the C mass, 52% of the H mass, and 49% of the N mass in OA (Fig. S5).

LV-OOA displays a pronounced diurnal cycle that is characterized by a gradual increase in concentration starting at ~09:00 a.m. and maximizing at ~17:00 p.m. (Fig. 13a). SV-OOA also starts to increase at ~09:00 a.m. but peaks at ~13:00 p.m. The decrease of SV-OOA in the afternoon is likely due to higher ambient temperature that evaporates more semi-volatile species, despite photochemical production of SOA. In addition, since this decrease of SV-OOA is accompanied with a gradual increase of LV-OOA, it is also possible that further oxidation of less oxidized, more-volatile SV-OOA to highly oxidized, less-volatile OA species has occurred. Indeed, the O/C ratio of total OOA gradually increases from 0.49 to 0.54 between 09:00 a.m. and 17:00 p.m. The continuous oxidation of SV-OOA to LV-OOA was observed at a remote coastal site as well (Hildebrandt et al., 2010).

3.5.2 Hydrocarbon-like OA (HOA)

The mass spectrum of HOA (Fig. 8e), which is characterized with the prominent $C_xH_{2x-1}^+$ and $C_xH_{2x+1}^+$ ion series, is very similar to previous reported reference spectra of POA emitted from gasoline and diesel combustion sources (Canagaratna et al., 2004; Schneider et al., 2006) and the spectra of HOA components determined at other sites (Zhang et al., 2005a; Aiken et al., 2009). The O/C (0.06) and OM/OC (1.24) ratios of HOA are also close to 0.03–0.04 and 1.22–1.24, respectively, determined for POA in motor vehicle exhaust (Mohr et al., 2009). As shown in Fig. 9e, HOA correlates best

with hydrocarbon ions $C_xH_{2x+1}^+$ and $C_xH_{2x-1}^+$. It contributes 25% of the $C_xH_y^+$ signal and only 3% of the $C_xH_yO_1^+$ and the $C_xH_yO_2^+$ signals (Fig. 10). In addition, HOA correlates well with combustion tracers such as EC (r^2=0.44) and NO_x (r^2=0.59) (Fig. 8e and Table 2) and presents a pronounced morning peak associated with the traffic emission (Fig. 13a). These facts together indicate that HOA is likely a surrogate for combustion POA, a conclusion achieved in a number of other studies (Zhang et al., 2005a,c; Aiken et al., 2009; Ulbrich et al., 2009). HOA on average accounts for 14.2% of the total OA mass for the whole campaign, showing the highest contribution (~28%) in the morning and the lowest (~8%) during the afternoon (Fig. 13b). As summarized in Table 2, the average ratios of HOA/EC (1.29) and HOA/NO_x (0.045 µg m^{-3} ppbv^{-1}) observed in this study are similar to previous observations in Pittsburgh (Zhang et al., 2005c) and Mexico City (Aiken et al., 2009).

3.5.3 Cooking OA (COA)

Although emissions related to cooking activities have been observed to contribute a significant fraction (~5–20%) of OA at various urban sites (Rogge et al., 1991; Zheng et al., 2002; Chow et al., 2007), reports of COA from AMS measurements are rare (Allan et al., 2010; Huang et al., 2010). In this study, a COA component was identified. The HRMS spectrum of COA is significantly different from those of other OA components but very similar to the reference spectra of POA from cooking emissions (Mohr et al., 2009) as well as the spectra of COA components observed in London (Allan et al., 2010) and Beijing (Huang et al., 2010).

The COA spectrum is characterized by a high ratio of m/z 55/57 (=2.9) and a high fraction of m/z 55 (f_{55}=8%), which could be used as a good diagnostics for the presence of COA at urban locations. As shown in Fig. 11, both m/z 55 and 57 have significant contributions from COA. In specific, COA contributes 38% and 29%, respectively, of $C_3H_3O^+$ and $C_4H_7^+$ at m/z 55, and 25% and 20%, respectively, of $C_3H_5O^+$ and $C_4H_9^+$ at m/z 57. In addition, COA shows most significant correlation with a few $C_xH_yO_1^+$ ions

Title Page

Abstract	Introduction
Conclusions	References
Tables	Figures

|◄ | ►|

◄ | ►

Back | Close

Full Screen / Esc

Printer-friendly Version

Interactive Discussion

(e.g., $C_5H_8O^+$, $C_6H_{10}O^+$, and $C_7H_{12}O^+$ in Fig. 9d), all of which are prominent peaks in the sources spectra of cooking emissions, thus could be used as spectral markers for COA.

The HRMS of COA reveals that it is on average more oxidized compared to HOA (O/C=0.18 vs. 0.06) and contains much higher contribution of oxygenated ions $C_xH_yO_1^+$ and $C_xH_yO_2^+$ (30% vs. ~9%). Figure S5 shows higher contribution of O to COA (10%) than to HOA (3%) as well, which is consistent with more oxygenated organic species found in meat cooking (Mohr et al., 2009). The O/C and H/C ratios of COA are 0.18 and 1.58, respectively (Fig. 8d). The diurnal cycle of COA is characterized by peaks corresponding to lunch and dinner times. Similar diurnal patterns of COA were observed in London (Allan et al., 2010) and Beijing (Huang et al., 2010). On average, COA accounts for 16% of the total OA mass, close to the values determined using the molecular tracer approach in Los Angeles (Rogge et al., 1991), Fresno, CA (Chow et al., 2007), and some urban sites in the southeastern United States (Zheng et al., 2002).

During this study, POA (=HOA+COA) accounts for an average 30.2% of the OA mass and up to ~40% during morning rush hour and at night (Fig. 13b). It is interesting to note that despite the fact that our sampling site is so close to two major highways (<1 mile), the average mass concentration of COA ($1.02\,\mu g/m^3$) is higher than that of HOA ($0.91\,\mu g/m^3$). This is an indication that cooking activities are a significant source of primary particles in NYC and that efforts to reduce particle pollution in this densely populated metropolitan area should focus on controlling both cooking and traffic emissions. POA and total OOA show almost no correlation (r^2=0.01, Fig. 12b), confirming their different source origins. However, there is a general trend that low particle loading periods are characterized with elevated POA and a high mass fraction of OA (Fig. 12b), due to stronger influences from local primary emissions. High PM events, on the other hand, are mainly contributed by secondary inorganic species and oxygenated organics species formed regionally.

Title Page

Abstract	Introduction
Conclusions	References
Tables	Figures

◄◄ ►►

◄ ►

Back Close

Full Screen / Esc

Printer-friendly Version

Interactive Discussion

3.5.4 Nitrogen-enriched OA (NOA)

A unique N-enriched OA (NOA) component was determined for this study. Compared to the other four OA components, it shows a much higher N/C ratio (0.053; Fig. 8c) and correlates much better with the N-containing ions (Fig. 9c). The NOA component correlates particularly tight ($r^2 > 0.85$) with $C_2H_4N^+$, $C_3H_8N^+$, and $C_4H_{10}N^+$, which were likely generated from amino compounds (McLafferty and Turecek, 1993). It, however, shows almost no correlation with $C_xH_y^+$ and $C_xH_yO_z^+$ (Fig. 9c). NOA on average accounts for 5.8% of the total OA mass, yet 39% of the $C_xH_yN_p^+$ signal (Fig. 10), and 33% of the nitrogen mass (Fig. S5).

The diurnal pattern of NOA is marked with a pronounced noon-time peak (Fig. 13a). Note that a "local N-containing reduced OA" (LOA) component (N/C=0.06) was observed in Mexico City (Aiken et al., 2009), but its mass spectrum and diurnal pattern are significantly different from the NOA component resolved in this study. The mass spectrum of NOA resembles more to that of OOA, while LOA in Mexico City is more similar to HOA and biomass burning OA (BBOA). The O/C and OM/OC ratios of NOA are 0.37 and 1.69, respectively, which are close to those of SV-OOA but much higher than 0.13 and 1.40, respectively, of LOA in Mexico City. These together indicate that the NOA observed in NYC is different from the LOA detected in Mexico City.

Elevated NOA concentrations frequently occur around noon (Fig. 8c) in association with southerly wind (Fig. 14a). To investigate the sources and processes of NOA, periods with large NOA peaks (∼17% of time) are classified as high NOA events (Hi-NOA) while the rest of the time as Lo-NOA. The average concentration of NOA during Hi-NOA ($1.29\,\mu g/m^3$) is ∼6 times higher than during Lo-NOA ($0.22\,\mu g/m^3$). Note that the average NR-PM$_1$ composition is very similar between the two types of periods except for a substantially higher fraction of NOA during Hi-NOA. Based on comparing measured NH_4^+ vs. predicted NH_4^+ ($=18\times(SO_4^{2-}/48+NO_3^-/62+Cl^-/35.5)$; Zhang et al., 2007b), aerosol particles appear to be slightly anion-rich during Hi-NOA while fully neutralized during Lo-NOA (Fig. 14b), suggesting NOA might be carrying positive charges. In

addition, Fig. 14c illustrates a broader size distribution of *m/z* 58, which is the *m/z* that is contributed the most by NOA (Fig. 11e), during Hi-NOA than during Lo-NOA while the size distributions of both *m/z* 44 and 57 show essentially no difference. Other *m/z*'s with relatively high contribution of N-containing ions such as *m/z* 42 ($C_2H_4N^+$) and 30 (CH_4N^+) also show broader size distributions during Hi-NOA. These results together suggest that organic nitrogen species such as amines might have played an important role in the atmospheric processing of OA, likely via acid-base chemistry, in NYC. A recent study in Cape Verde observed non-negligible contribution of aliphatic amines, e.g., dimethylamine (C_2H_7N) and diethylamine ($C_4H_{11}N$), to OC during algal blooms (Müller et al., 2009). Given the proximity of NYC to the Atlantic Ocean, it is possible that the NOA spikes are associated with marine emissions of aliphatic amines. In addition, given large industry emission sources over the southwest of NYC, industrial emissions could also be an important source of amines (Moffet et al., 2008).

3.6 Potential source regions of PM_1 in NYC

Figure 15a and Table S2 present the average composition of PM_1 and OA corresponding to four principal clusters of air masses, i.e., northwest (NW), west (W), southwest (SW), and Atlantic Ocean, respectively, determined via the trajectory cluster analysis of the HYSPLIT model. Aerosol loadings are on average lowest (6.6 µg/m^3) in the northwesterly air masses (cluster 1, 7.3% of time) and highest (14.1 µg/m^3) in the southwesterly air masses (cluster 4, 30.8% of time). These observations are consistent with the emission inventories of air pollutants in the northeastern United States (Fig. 15a). Significant differences in the chemical composition of PM_1 are also observed among different clusters, likely reflecting the characteristics of different source regions of air pollutants. The contributions of primary species (i.e., EC and HOA) to PM_1 (14.3%) and OA (33%) are the highest in the NW cluster, so is the fraction of OA (72% of PM_1). The low aerosol loadings are consistent with the average spatial distribution of AOD determined from satellite retrieval. As shown in Fig. 15b, the daily averaged AOD values observed above NYC correlate well the average PM_1 concentrations we measured

during this study. This is an indication that the average AOD distribution shown in Fig. 15c is likely a good representation of the spatial distribution of PM$_1$ during this study. These observations suggest that emissions of primary particles, primarily from local sources, play an important role controlling PM$_1$ concentration and loading in NYC during relatively clean periods. Comparatively, secondary species, e.g., OOA and sulfate, dominate the PM$_1$ composition with air masses originated from SW. The westerly air masses (cluster 2, 37.3% of time) also correlate with high aerosol pollution with large fraction of secondary species. The observed correlations between aerosol loading and air mass trajectories are consistent with the high AOD and the large source emissions in the regions W and SW to NYC, e.g., large coal-fired plants and industrial sources in the Ohio River Valley, West Virginia, and Pennsylvania (Polissar et al., 2001; Qin et al., 2006). For ∼25% of the time during this study, air masses were traced back to the Atlantic Ocean (cluster 3) with very low flow speed. Relatively high loadings of PM$_1$ composed of higher fraction of sulfate (26.6% of PM$_1$) and LV-OOA (40% of OA) appear to correlate with these air masses, which likely reflects the influences due to the recirculation of the outflow of polluted air from the U.S. continent. Indeed, the high AOD along the coastal line and near shore (Fig. 15c) corroborates this hypothesis.

4 Conclusions

The mass concentration, chemical composition, and size distributions of submicron aerosol species in NYC were measured in-situ using a HR-AMS in summer 2009. Aerosol composition varies dynamically with OA and sulfate comprising the major fraction of total PM$_1$ mass, on average accounting for 54% and 24%, respectively. Analysis of aerosol ion balance indicates that submicron particles in NYC are overall bulk neutralized. The size distributions of NR-PM$_1$ species, all of which vary dynamically during this study, on average present a similar large accumulation mode peaking at ∼550 nm with an additional small particle mode (∼150 nm) for OA. In addition to boundary layer dynamics, local photochemical production plays an important role in controlling the

variation of sulfate and OA during daytime, while gas-to-particle partitioning drives the diurnal cycle of nitrate. Elemental analysis presents an average O/C and OM/OC ratio of 0.36($\pm$0.08) and 1.62($\pm$0.11), respectively for OA.

PMF analysis of the HRMS of OA has identified five components, i.e., a traffic-related HOA, a highly aged, regional LV-OOA, a less oxidized, fresher and more volatile SV-OOA, a cooking-related COA, and a NOA enriched of organic nitrogen compounds. SV-OOA and LV-OOA constitute the largest fraction of OA, accounting for 34% and 30%, respectively, on average. HOA and COA account for another 14% and 16% of the OA mass, respectively. HOA correlates well with the primary traffic emission tracers, with HOA/EC and HOA/NO$_x$ ratios being 1.29 and 0.045 (μg m^{-3} ppbv^{-1}), respectively. LV-OOA correlates tightly with sulfate and C$_x$H$_y$O$_2^+$ ions while SV-OOA correlates with chloride and C$_x$H$_y$O$_1^+$ ions. The diurnal cycle of HOA shows a pronounced morning traffic peak, consistent with those of EC and NO$_x$. The diurnal cycles of SV-OOA and LV-OOA demonstrate a trend of chemical evolution of SOA in NYC involving a continuum of oxidation from SV-OOA to LV-OOA, which is consistent with a gradual increase of O/C ratio and a corresponding decrease of H/C ratio. The diurnal cycle of COA shows two pronounced peaks, corresponding to lunch and dinner times. NOA, which accounts for 5.8% of the OA mass, yet 33% of the organic N mass, shows a pronounced peak around noon time and correlates well with amines related peaks, e.g., C$_x$H$_{2x+2}$N$^+$. Analysis of the sources and ion balance of NOA suggests that N-containing organic species such as amines might have played an important role in the atmospheric processing of OA, likely via acid-base chemistry. Air mass trajectory analysis, together with satellite AOD observations, indicates that emissions of primary particles from local sources likely play an important role controlling PM$_1$ concentration and loading in NYC during relatively clean periods associated with the northwesterly flow. High PM pollution events, however, are mainly contributed by secondary inorganic and organic particles typically associated with air masses originated from regions to the west and southwest of the city.

Appendix A

A1   Estimation of production rates of HNO_3 and H_2SO_4

The production rate of HNO_3 and H_2SO_4 can be estimated from bi-molecule association reactions (Seinfeld and Pandis, 2006). The effective second-order rate constant for a given temperature and pressure (altitude) can be calculated using Eq. (A1).

$$k([M],T) = \left(\frac{k_0(T)[M]}{1 + \frac{k_0(T)[M]}{k_\infty(T)}} \right) 0.6^{\left\{ 1 + \left[\log\left(\frac{k_0(T)[M]}{k_\infty[M]} \right) \right] \right\}} (cm^6 molecule^{-2} s^{-1}) \tag{A1}$$

$$k_0(T) = k_0^{300} \left(\frac{T}{300} \right)^{-n} (cm^6 molecule^{-2} s^{-1}) \tag{A2}$$

$$k_\infty(T) = k_\infty^{300} \left(\frac{T}{300} \right)^{-m} (cm^3 molecule^{-1} s^{-1}) \tag{A3}$$

$$NO_2 + OH \xrightarrow{M} HONO_2 \tag{A4}$$

$$SO_2 + OH \xrightarrow{M} HOSO_2 \tag{A5}$$

Where $k_0(T)$ (Eq. A2) is low-pressure-limiting rate constant and $k_\infty(T)$ is the high-pressure-limiting rate constant. The four parameters k_0^{300}, n, k_∞^{300}, and m for Eqs. (A2) and (A3) are listed in Table A1.

A2   Calculation of the equilibrium constant of gas-to-particle partitioning

Formation of ammonium nitrate involves an equilibrium reaction between the gas phase NH_3 and HNO_3, and particle phase NH_4NO_3 (React. A6). The gas-to-particle partition-

Title Page

Abstract | Introduction

Conclusions | References

Tables | Figures

|◀ | ▶|

◀ | ▶

Back | Close

Full Screen / Esc

Printer-friendly Version

Interactive Discussion

ing is strongly temperature dependent, and the equilibrium constant of React. (A6) can be calculated as Eq. (A7) (Seinfeld and Pandis, 2006)

$$NH_3(g) + HNO_3(g) \longleftrightarrow NH_4NO_3(s) \tag{A6}$$

$$k(T) = k(298) \exp\left\{ a\left(\frac{298}{T} - 1\right) + b\left[1 + \ln\left(\frac{298}{T}\right) - \frac{298}{T}\right]\right\}, \tag{A7}$$

where T is the ambient temperature in Kelvin. $k(298) = 3.35 \times 10^{16}$ atm^{-2}, $a = 75.11$, and $b = -13.5$.

Supplementary material related to this article is available online at: http://www.atmos-chem-phys-discuss.net/10/22669/2010/ acpd-10-22669-2010-supplement.pdf.

References

Aiken, A. C., DeCarlo, P. F., Kroll, J. H., et al.: O/C and OM/OC ratios of primary, secondary, and ambient organic aerosols with high-resolution time-of-flight aerosol mass spectrometry, Environ. Sci. Technol., 42, 4478–4485, 2008.

Aiken, A. C., Salcedo, D., Cubison, M. J., Huffman, J. A., DeCarlo, P. F., Ulbrich, I. M., Docherty, K. S., Sueper, D., Kimmel, J. R., Worsnop, D. R., Trimborn, A., Northway, M., Stone, E. A., Schauer, J. J., Volkamer, R. M., Fortner, E., de Foy, B., Wang, J., Laskin, A., Shutthanandan, V., Zheng, J., Zhang, R., Gaffney, J., Marley, N. A., Paredes-Miranda, G., Arnott, W. P., Molina, L. T., Sosa, G., and Jimenez, J. L.: Mexico City aerosol analysis during MILAGRO using high resolution aerosol mass spectrometry at the urban supersite (T0) – Part 1: Fine particle composition and organic source apportionment, Atmos. Chem. Phys., 9, 6633–6653, doi:10.5194/acp-9-6633-2009, 2009.

Alfarra, M. R., Coe, H., Allan, J. D., et al.: Characterization of urban and regional organic aerosols in the Lower Fraser Valley using two aerodyne aerosol mass spectrometers, Atmos. Environ., 38, 5745–5758, 2004.

Allan, J. D., Alfarra, M. R., Bower, K. N., et al.: Quantitative sampling using an aerodyne aerosol mass spectrometer. Part 2: measurements of fine particulate chemical composition in two UK Cities, J. Geophys. Res.-Atmos., 108, 4091, doi:4010.1029/2002JD002359, 2003a.

Allan, J. D., Jimenez, J. L., Williams, P. I., et al.: Quantitative sampling using an aerodyne aerosol mass spectrometer. Part 1: techniques of data interpretation and error analysis, J. Geophys. Res.-Atmos., 108, 4090, doi:4010.1029/2002JD002358, 2003b.

Allan, J. D., Williams, P. I., Morgan, W. T., Martin, C. L., Flynn, M. J., Lee, J., Nemitz, E., Phillips, G. J., Gallagher, M. W., and Coe, H.: Contributions from transport, solid fuel burning and cooking to primary organic aerosols in two UK cities, Atmos. Chem. Phys., 10, 647–668, doi:10.5194/acp-10-647-2010, 2010.

Association, A. L.: State of the Air 2010, American Lung Association, available at: http://www.lungusa.org, 2010.

Bae, M.-S., Demerjian, K. L., and Schwab, J. J.: Seasonal estimation of organic mass to organic carbon in $PM_{2.5}$ at rural and urban locations in New York state, Atmos. Environ., 40, 7467–7479, 2006.

Canagaratna, M., Jayne, J., Jimenez, J. L., et al.: Chemical and microphysical characterization of aerosols via aerosol mass spectrometry, Mass Spectrom. Rev., 26, 185–222, 2007.

Canagaratna, M. R., Jayne, J. T., Ghertner, D. A., et al.: Chase studies of particulate emissions from in-use New York City vehicles, Aerosol Sci. Tech., 38, 555–573, 2004.

Chow, J. C., Watson, J. G., Lowenthal, D. H., Chen, L. W. A., Zielinska, B., Mazzoleni, L. R., and Magliano, K. L.: Evaluation of organic markers for chemical mass balance source apportionment at the Fresno Supersite, Atmos. Chem. Phys., 7, 1741–1754, doi:10.5194/acp-

Characterization of organic and inorganic aerosols in New York City

Y.-L. Sun et al.

7-1741-2007, 2007.

DeCarlo, P. F., Kimmel, J. R., Trimborn, A., et al.: Field-deployable, high-resolution, time-of-flight aerosol mass spectrometer, Anal. Chem., 78, 8281–8289, 2006.

DeCarlo, P. F., Dunlea, E. J., Kimmel, J. R., Aiken, A. C., Sueper, D., Crounse, J., Wennberg, P. O., Emmons, L., Shinozuka, Y., Clarke, A., Zhou, J., Tomlinson, J., Collins, D. R., Knapp, D., Weinheimer, A. J., Montzka, D. D., Campos, T., and Jimenez, J. L.: Fast airborne aerosol size and chemistry measurements above Mexico City and Central Mexico during the MILA-GRO campaign, Atmos. Chem. Phys., 8, 4027–4048, doi:10.5194/acp-8-4027-2008, 2008.

DeCarlo, P. F., Ulbrich, I. M., Crounse, J., de Foy, B., Dunlea, E. J., Aiken, A. C., Knapp, D., Weinheimer, A. J., Campos, T., Wennberg, P. O., and Jimenez, J. L.: Investigation of the sources and processing of organic aerosol over the Central Mexican Plateau from aircraft measurements during MILAGRO, Atmos. Chem. Phys., 10, 5257–5280, doi:10.5194/acp-10-5257-2010, 2010.

Demerjian, K. L. and Mohnen, V. A.: Synopsis of the temporal variation of particulate matter composition and size, J. Air Waste Manage. Assoc., 58, 216–233, 2008.

Draxler, R. R. and Rolph, G. D.: HYSPLIT (HYbrid Single-Particle Lagrangian Integrated Tra-jectory) Model access via NOAA ARL READY Website, NOAA Air Resources Laboratory, Silver Spring, MD, available at: http://www.arl.noaa.gov/ready/hysplit4.html, 2003.

Drewnick, F., Schwab, J. J., Hogrefe, O., et al.: Intercomparison and evaluation of four semi-continuous PM$_{2.5}$ sulfate instruments, Atmos. Environ., 37, 3335–3350, 2003.

Drewnick, F., Schwab, J. J., Jayne, J. T., et al.: Measurement of ambient aerosol composition during the PMTACS-NY 2001 using an aerosol mass spectrometer. Part I: mass concentra-tions, Aerosol Sci. Tech., 38, 92–103, 2004a.

Drewnick, F., Schwab, J. J., Jayne, J. T., et al.: Measurement of ambient aerosol composi-tion during the PMTACS-NY 2001 using an aerosol mass spectrometer. Part II: chemically speciated mass distributions, Aerosol Sci. Tech., 38, 104–117, 2004b.

Drewnick, F., Hings, S. S., DeCarlo, P. F., et al.: A new time-of-flight aerosol mass spectrometer (ToF-AMS) – instrument description and first field deployment, Aerosol Sci. Tech., 39, 637–658, 2005.

Dutkiewicz, V. A., Qureshi, S., Khan, A. R., et al.: Sources of fine particulate sulfate in New York, Atmos. Environ., 38, 3179–3189, 2004.

Dutkiewicz, V. A., Qureshi, S., Husain, L., Schwab, J. J., and Demerjian, K. L.: Elemental composition of PM$_{2.5}$ aerosols in Queens, New York: evaluation of sources of fine-particle

mass, Atmos. Environ., 40, 347–359, 2006.

Eatough, D. J., Long, R. W., Modey, W. K., and Eatough, N. L.: Semi-volatile secondary organic aerosol in urban atmospheres: meeting a measurement challenge, Atmos. Environ., 37, 1277–1292, 2003.

5 Hildebrandt, L., Engelhart, G. J., Mohr, C., Kostenidou, E., Lanz, V. A., Bougiatioti, A., De-Carlo, P. F., Prevot, A. S. H., Baltensperger, U., Mihalopoulos, N., Donahue, N. M., and Pandis, S. N.: Aged organic aerosol in the Eastern Mediterranean: the Finokalia Aerosol Measurement Experiment – 2008, Atmos. Chem. Phys., 10, 4167–4186, doi:10.5194/acp-10-4167-2010, 2010.

10 Huang, X.-F., He, L.-Y., Hu, M., Canagaratna, M. R., Sun, Y., Zhang, Q., Zhu, T., Xue, L., Zeng, L.-W., Liu, X.-G., Zhang, Y.-H., Jayne, J. T., Ng, N. L., and Worsnop, D. R.: Highly time-resolved chemical characterization of atmospheric submicron particles during 2008 Beijing Olympic Games using an Aerodyne High-Resolution Aerosol Mass Spectrometer, Atmos. Chem. Phys., 10, 8933–8945, doi:10.5194/acp-10-8933-2010, 2010.

15 Huffman, J. A., Jayne, J. T., Drewnick, F., et al.: Design, modeling, optimization, and experimental tests of a particle beam width probe for the aerodyne aerosol mass spectrometer, Aerosol Sci. Tech., 39, 1143–1163, 2005.

IPCC: Summary for policymakers, in: Climate Change 2007: The Physical Science Basis. Contribution of Working Group I to the Fourth Assessment Report of the Intergovernmental Panel
20 on Climate Change, edited by: Solomon, S., Qin, D., Manning, M., Chen, Z., Marquis, M., Averyt, K. B., Tignor, M., and Miller, H. L., Cambridge University Press, Cambridge, UK and New York, NY, USA, 2007.

Jayne, J. T., Leard, D. C., Zhang, X., et al.: Development of an aerosol mass spectrometer for size and composition analysis of submicron particles, Aerosol Sci. Tech., 33, 49–70, 2000.

25 Jimenez, J. L., Jayne, J. T., Shi, Q., et al.: Ambient aerosol sampling with an aerosol mass spectrometer, J. Geophys. Res.-Atmos., 108, 8425, doi:8410:1029/2001JD001213, 2003.

Jimenez, J. L., Canagaratna, M. R., Donahue, N. M., et al.: Evolution of organic aerosols in the atmosphere, Science, 326, 1525–1529, doi:10.1126/science.1180353, 2009.

JPL: Chemical Kinetics and Photochemical Data for Use in Atmospheric Studies Evaluation
30 Number 16, Jet Propulsion Laboratory, Pasadena, CA, 2009.

Kanakidou, M., Seinfeld, J. H., Pandis, S. N., Barnes, I., Dentener, F. J., Facchini, M. C., Van Dingenen, R., Ervens, B., Nenes, A., Nielsen, C. J., Swietlicki, E., Putaud, J. P, Balkanski, Y., Fuzzi, S., Horth, J., Moortgat, G. K., Winterhalter, R., Myhre, C. E. L., Tsigaridis, K.,

Characterization of organic and inorganic aerosols in New York City

Y.-L. Sun et al.

Vignati, E., Stephanou, E. G., and Wilson, J.: Organic aerosol and global climate modelling: a review, Atmos. Chem. Phys., 5, 1053–1123, doi:10.5194/acp-5-1053-2005, 2005.

Kondo, Y., Miyazaki, Y., Takegawa, N., et al.: Oxygenated and water-soluble organic aerosols in Tokyo, J. Geophys. Res., 112, D01203, doi:01210.01029/02006JD007056, 2006.

5   Lall, R. and Thurston, G. D.: Identifying and quantifying transported vs. local sources of New York City $PM_{2.5}$ fine particulate matter air pollution, Atmos. Environ., 40, 333–346, 2006.

Lanz, V. A., Alfarra, M. R., Baltensperger, U., Buchmann, B., Hueglin, C., and Prévôt, A. S. H.: Source apportionment of submicron organic aerosols at an urban site by factor analytical modelling of aerosol mass spectra, Atmos. Chem. Phys., 7, 1503–1522, doi:10.5194/acp-7-

10   1503-2007, 2007.

Massoli, P., Jayne, J., Fortner, E., et al.: Temporal-spatial evolution and chemical characterization of particulate matter from vehicular exhaust near major roadways: results from the 2009 Queens College Air Quality study, AAAR 2010 Specialty Conference, San Diego, California, Abstract Number: 388, 2010.

15   McLafferty, F. W. and Turecek, F.: Interpretation of Mass Spectra, University Science Books, Mill Valley, California, 1993.

Moffet, R. C., de Foy, B., Molina, L. T., Molina, M. J., and Prather, K. A.: Measurement of ambient aerosols in northern Mexico City by single particle mass spectrometry, Atmos. Chem. Phys., 8, 4499–4516, doi:10.5194/acp-8-4499-2008, 2008.

20   Mohr, C., Huffman, J. A., Cubison, M. J., et al.: Characterization of primary organic aerosol emissions from meat cooking, trash burning, and motor vehicles with High-Resolution Aerosol Mass Spectrometry and comparison with ambient and chamber observations, Environ. Sci. Technol., 43, 2443–2449, doi:10.1021/es8011518, 2009.

Molina, M. J. and Molina, L. T.: Megacities and atmospheric pollution, J. Air Waste Manage.

25   Assoc., 54, 644–680, 2004.

Morgan, W. T., Allan, J. D., Bower, K. N., Highwood, E. J., Liu, D., McMeeking, G. R., Northway, M. J., Williams, P. I., Krejci, R., and Coe, H.: Airborne measurements of the spatial distribution of aerosol chemical composition across Europe and evolution of the organic fraction, Atmos. Chem. Phys., 10, 4065–4083, doi:10.5194/acp-10-4065-2010, 2010.

30   Müller, C., Iinuma, Y., Karstensen, J., van Pinxteren, D., Lehmann, S., Gnauk, T., and Herrmann, H.: Seasonal variation of aliphatic amines in marine sub-micrometer particles at the Cape Verde islands, Atmos. Chem. Phys., 9, 9587–9597, doi:10.5194/acp-9-9587-2009, 2009.

Characterization of organic and inorganic aerosols in New York City

Y.-L. Sun et al.

Title Page

Abstract	Introduction
Conclusions	References
Tables	Figures

◄◄   ►►

◄   ►

Back   Close

Full Screen / Esc

Printer-friendly Version

Interactive Discussion

Ng, N. L., Canagaratna, M. R., Zhang, Q., Jimenez, J. L., Tian, J., Ulbrich, I. M., Kroll, J. H., Docherty, K. S., Chhabra, P. S., Bahreini, R., Murphy, S. M., Seinfeld, J. H., Hildebrandt, L., Donahue, N. M., DeCarlo, P. F., Lanz, V. A., Prévôt, A. S. H., Dinar, E., Rudich, Y., and Worsnop, D. R.: Organic aerosol components observed in Northern Hemispheric datasets from Aerosol Mass Spectrometry, Atmos. Chem. Phys., 10, 4625–4641, doi:10.5194/acp-10-4625-2010, 2010.

Paatero, P., and Tapper, U.: Positive matrix factorization: a non-negative factor model with optimal utilization of error estimates of data values, Environmetrics, 5, 111–126, 1994.

Paatero, P. and Hopke, P. K.: Discarding or downweighting high-noise variables in factor analytic models, Anal. Chim. Acta, 490, 277–289, 2003.

Polissar, A. V., Hopke, P. K., and Poirot, R. L.: Atmospheric aerosol over Vermont: chemical composition and sources, Environ. Sci. Technol., 35, 4604–4621, 2001.

Pope, C. A., Burnett, R. T., Thun, M. J., et al.: Lung cancer, cardiopulmonary mortality, and long-term exposure to fine particulate air pollution, JAMA-J. Am. Med. Assoc., 287, 1132–1141, 2002.

Pope, C. A., III, Ezzati, M., and Dockery, D. W.: Fine-particulate air pollution and life expectancy in the United States, N. Engl. J. Med., 360, 376–386, doi:10.1056/NEJMsa0805646, 2009.

Qin, Y., Kim, E., and Hopke, P. K.: The concentrations and sources of $PM_{2.5}$ in metropolitan New York City, Atmos. Environ., 40, 312–332, 2006.

Rattigan, O. V., Felton, H. D., Bae, M.-S., Schwab, J. J., and Demerjian, K. L.: Multi-year hourly $PM_{2.5}$ carbon measurements in New York: diurnal, day of week and seasonal patterns, Atmos. Environ., 44, 2043–2053, 2010.

Remer, L. A., Kaufman, Y. J., Tanré, D., et al.: The MODIS aerosol algorithm, products, and validation, J. Atmos. Sci., 62, 947–973, doi:10.1175/JAS3385.1, 2005.

Ren, X., Harder, H., Martinez, M., et al.: HO_x concentrations and OH reactivity observations in New York City during PMTACS-NY2001, Atmos. Environ., 37, 3627–3637, 2003.

Rogge, W. F., Hildemann, L. M., Mazurek, M. A., Cass, G. R., and Simonelt, B. R. T.: Sources of fine organic aerosol. 1. Charbroilers and meat cooking operations, Environ. Sci. Technol., 25, 1112–1125, 1991.

Salcedo, D., Onasch, T. B., Dzepina, K., Canagaratna, M. R., Zhang, Q., Huffman, J. A., DeCarlo, P. F., Jayne, J. T., Mortimer, P., Worsnop, D. R., Kolb, C. E., Johnson, K. S., Zuberi, B., Marr, L. C., Volkamer, R., Molina, L. T., Molina, M. J., Cardenas, B., Bernabé, R. M., Márquez, C., Gaffney, J. S., Marley, N. A., Laskin, A., Shutthanandan, V., Xie, Y., Brune, W.,

Title Page

Abstract | Introduction

Conclusions | References

Tables | Figures

◄◄ | ►►

◄ | ►

Back | Close

Full Screen / Esc

Printer-friendly Version

Interactive Discussion

Lesher, R., Shirley, T., and Jimenez, J. L.: Characterization of ambient aerosols in Mexico City during the MCMA-2003 campaign with Aerosol Mass Spectrometry: results from the CENICA Supersite, Atmos. Chem. Phys., 6, 925–946, doi:10.5194/acp-6-925-2006, 2006.

Salcedo, D., Onasch, T. B., Aiken, A. C., Williams, L. R., de Foy, B., Cubison, M. J., Worsnop, D. R., Molina, L. T., and Jimenez, J. L.: Determination of particulate lead using aerosol mass spectrometry: MILAGRO/MCMA-2006 observations, Atmos. Chem. Phys., 10, 5371–5389, doi:10.5194/acp-10-5371-2010, 2010.

Schneider, J., Weimer, S., Drewnick, F., et al.: Mass spectrometric analysis and aerodynamic properties of various types of combustion-related aerosol particles, Int. J. Mass Spectrom., 258, 37–49, 2006.

Schwab, J. J., Felton, H. D., and Demerjian, K. L.: Aerosol chemical composition in New York state from integrated filter samples: urban/rural and seasonal contrasts, J. Geophys. Res., 109, D16S05, doi:10.1029/2003jd004078, 2004.

Schwab, J. J., Bae, M.-S., Demerjian, K., et al.: A Mobile Laboratory for On-Road and Near-Roadway Measurements of Fine Particulate Matter and Pollutant Gases, AAAR 2010 Specialty Conference, San Diego, California, Abstract 7SQ3.T2.101, 2010.

Seinfeld, J. H. and Pandis, S. N.: Atmospheric Chemistry and Physics: From Air Pollution to Climate Change, Wiley, John & Sons, Incorporated, New York, 1203 pp., 2006.

Sorooshian, A., Brechtel, F. J., Ma, Y., et al.: Modeling and characterization of a Particle-into-Liquid Sampler (PILS), Aerosol Sci. Tech., 40, 396–409, 2006.

Sueper, D.: ToF-AMS Analysis Software, available at: http://cires.colorado.edu/jimenez-group/ToFAMSResources/ToFSoftware/index.html, 2010.

Sun, J., Zhang, Q., Canagaratna, M. R., et al.: Highly time- and size-resolved characterization of submicron aerosol particles in Beijing using an aerodyne aerosol mass spectrometer, Atmos. Environ., 44, 131–140, 2010.

Sun, Y., Zhang, Q., Macdonald, A. M., Hayden, K., Li, S. M., Liggio, J., Liu, P. S. K., Anlauf, K. G., Leaitch, W. R., Steffen, A., Cubison, M., Worsnop, D. R., van Donkelaar, A., and Martin, R. V.: Size-resolved aerosol chemistry on Whistler Mountain, Canada with a high-resolution aerosol mass spectrometer during INTEX-B, Atmos. Chem. Phys., 9, 3095–3111, doi:10.5194/acp-9-3095-2009, 2009.

Sunder Raman, R., Hopke, P. K., and Holsen, T. M.: Carbonaceous aerosol at two rural locations in New York State: characterization and behavior, J. Geophys. Res.-Atmos., 113, D12202, doi:12210.11029/12007JD009281, 2008.

Characterization of organic and inorganic aerosols in New York City

Y.-L. Sun et al.

Title Page

Abstract	Introduction
Conclusions	References
Tables	Figures

◄◄   ►►

◄   ►

Back   Close

Full Screen / Esc

Printer-friendly Version

Interactive Discussion

Takegawa, N., Miyazaki, Y., Kondo, Y., et al.: Characterization of an aerodyne aerosol mass spectrometer (AMS): intercomparison with other aerosol Instruments, Aerosol Sci. Tech., 39, 760–770, 2005.

Takegawa, N., Miyakawa, T., Kondo, Y., et al.: Seasonal and diurnal variations of submicron organic aerosols in Tokyo observed using the aerodyne aerosol mass spectrometer (AMS), J. Geophys. Res., 111, D11206, doi:10.1029/2005JD006515, 2006.

Turpin, B. J. and Lim, H. J.: Species contributions to $PM_{2.5}$ mass concentrations: revisiting common assumptions for estimating organic mass, Aerosol Sci. Tech., 35, 602–610, 2001.

Ulbrich, I. M., Canagaratna, M. R., Zhang, Q., Worsnop, D. R., and Jimenez, J. L.: Interpretation of organic components from Positive Matrix Factorization of aerosol mass spectrometric data, Atmos. Chem. Phys., 9, 2891–2918, doi:10.5194/acp-9-2891-2009, 2009.

Venkatachari, P., Zhou, L., Hopke, P. K., et al.: Spatial and temporal variability of black carbon in New York City, J. Geophys. Res., 111, D10S05, doi:10.1029/2005jd006314, 2006.

Volkamer, R., Jimenez, J. L., Martini, F. S., et al.: Secondary organic aerosol formation from anthropogenic VOCs: rapid and higher than expected, Geophys. Res. Lett., 33, L17811, doi:10.1029/2006GL026899, 2006.

Weimer, S., Drewnick, F., Hogrefe, O., et al.: Size-selective nonrefractory ambient aerosol measurements during the particulate matter technology assessment and characterization study – New York 2004 winter intensive in New York City, J. Geophys. Res., 111, D18305, doi:10.1029/2006JD007215, 2006.

Wexler, A. S. and Johnston, M. V.: What have we learned from highly time resolved measurements during the EPA supersite program and related studies?, J. Air Waste Manage. Assoc., 58, 303–319, 2008.

Zhang, Q., Alfarra, M. R., Worsnop, D. R., et al.: Deconvolution and quantification of hydrocarbon-like and oxygenated organic aerosols based on aerosol mass spectrometry, Environ. Sci. Technol., 39, 4938–4952, doi:4910.1021/es048568l, 2005a.

Zhang, Q., Canagaratna, M. C., Jayne, J. T., Worsnop, D. R., and Jimenez, J. L.: Time and size-resolved chemical composition of submicron particles in Pittsburgh – implications for aerosol sources and processes, J. Geophys. Res., 110, D07S09, doi:10.1029/2004JD004649, 2005b.

Zhang, Q., Worsnop, D. R., Canagaratna, M. R., and Jimenez, J. L.: Hydrocarbon-like and oxygenated organic aerosols in Pittsburgh: insights into sources and processes of organic aerosols, Atmos. Chem. Phys., 5, 3289–3311, doi:10.5194/acp-5-3289-2005, 2005c.

Zhang, Q., Jimenez, J. L., Canagaratna, M. R., et al.: Ubiquity and dominance of oxygenated species in organic aerosols in anthropogenically-influenced Northern Hemisphere mid-latitudes, Geophys. Res. Lett., 34, L13801, doi:13810.11029/12007GL029979, 2007a.

Zhang, Q., Jimenez, J. L., Worsnop, D. R., and Canagaratna, M.: A case study of urban particle acidity and its effect on secondary organic aerosol, Environ. Sci. Technol., 41, 3213–3219, 2007b.

Zheng, M., Cass, G. R., Schauer, J. J., and Edgerton, E. S.: Source apportionment of $PM_{2.5}$ in the Southeastern United States using solvent-extractable organic compounds as tracers, Environ. Sci. Technol., 36, 2361–2371, 2002.

Title Page

Abstract | Introduction

Conclusions | References

Tables | Figures

◄ | ►

◄ | ►

Back | Close

Full Screen / Esc

Printer-friendly Version

Interactive Discussion

Table 1. Summary of the mass concentrations ($\mu g/m^3$) of NR-PM$_1$ species, OA components, and EC.

	Average	1σ	Median	Minimum	Maximum
Organics	6.34	3.20	5.76	1.03	27.7
LV-OOA	1.93	1.38	1.72	0.06	7.63
SV-OOA	2.14	1.86	1.66	0.04	8.83
NOA	0.37	0.55	0.76	0.00	3.66
COA	1.02	0.96	0.63	0.01	5.61
HOA	0.91	0.91	0.21	0.08	6.54
Sulfate	2.82	1.81	2.71	0.13	12.1
Nitrate	0.49	0.54	0.33	0.03	4.44
Ammonium	1.28	0.73	1.25	0.06	3.67
Chloride	0.03	0.03	0.02	<D.L.[a]	0.20
EC	0.70	0.54	0.57	<D.L.	6.21
Total[b]	11.7	5.43	11.1	2.08	35.8

[a] Detection Limit.
[b] Total=organics+sulfate+nitrate+ammonium+chloride+EC.

ACPD

10, 22669–22723, 2010

Characterization of organic and inorganic aerosols in New York City

Y.-L. Sun et al.

Title Page

Abstract | Introduction

Conclusions | References

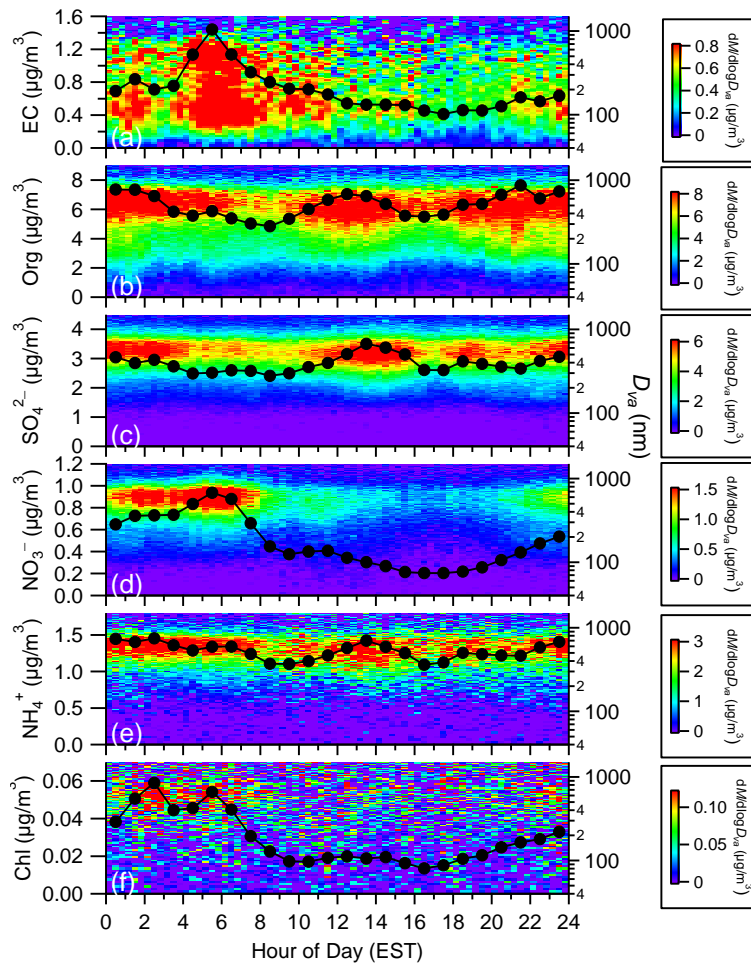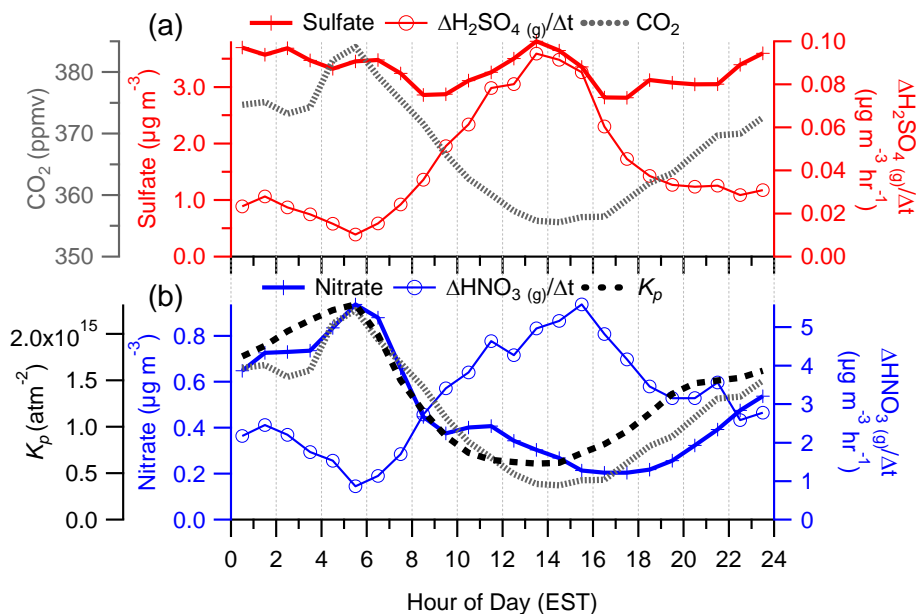Tables | Figures

◄ | ►

◄ | ►

Back | Close

Full Screen / Esc

Printer-friendly Version

Interactive Discussion

Characterization of organic and inorganic aerosols in New York City

Y.-L. Sun et al.

Title Page

Abstract | Introduction

Conclusions | References

Tables | Figures

◄ | ►►

◄ | ►

Back | Close

Full Screen / Esc

Printer-friendly Version

Interactive Discussion

Table 2. Correlations between OA components and tracers from collocated measurements.

	r^2	Slope		r^2	Slope
HOA vs. EC	0.44	1.29^a	SV-OOA vs. Chloride	0.30	48.9^a
	0.72	1.41^b	Total OOA vs. Sulfate	0.51	1.29^a
	0.65	1.25^c		0.74	0.38^b
HOA vs. NO_x	0.59	0.045^a	Total OOA vs. O_x	0.08	0.11^a
	0.82	0.042^b		0.55	0.12^d
LV-OOA vs. Sulfate	0.66	0.65^a			

[a] NYC, this study.
[b] Pittsburgh (Zhang et al., 2005c).
[c] BC, Mexico City (Aiken et al., 2009).
[d] Mexico City, (Aiken et al., 2009).

Title Page

Abstract | Introduction

Conclusions | References

Tables | Figures

◀ | ▶

◀ | ▶

Back | Close

Full Screen / Esc

Printer-friendly Version

Interactive Discussion

Table A1. Kinetic parameters used to determine the production rates of HNO_3 and H_2SO_4 (JPL, 2009).

	k_0^{300}	n	k_∞^{300}	m
$NO_2+OH\xrightarrow{M}HONO_2$	2.0×10^{-30}	3.0	2.5×10^{-11}	0
$SO_2+OH\xrightarrow{M}HOSO_2$	3.0×10^{-31}	3.3	1.5×10^{-12}	0
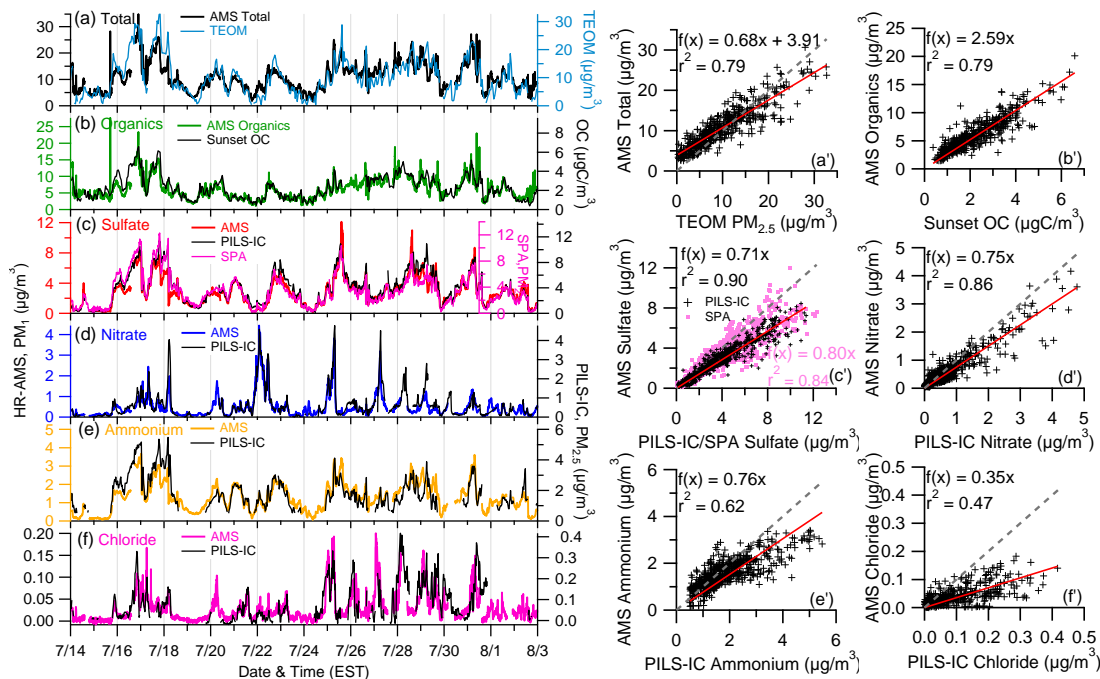
Fig. 1. Inter-comparisons between the NR-PM$_1$ mass concentrations measured by the HR-ToF-AMS versus the data acquired by collocated instruments: **(a)** total (=organics+sulfate+nitrate+ammonium+chloride) vs. PM$_{2.5}$ mass by a TEOM, **(b)** organics vs. PM$_{2.5}$ OC by a Sunset Lab OC/EC Analyzer, and **(c–f)** sulfate, nitrate, ammonium, and chloride vs. those measured by a PILS-IC. (c) also shows the comparison with PM$_{2.5}$ sulfate by a SPA. (a'–f') are the scatter plots with the linear regression parameters and the 1:1 line (dash line) shown for the comparisons.

Title Page

Abstract | Introduction

Conclusions | References

Tables | Figures

|◄ | ►|

◄ | ►
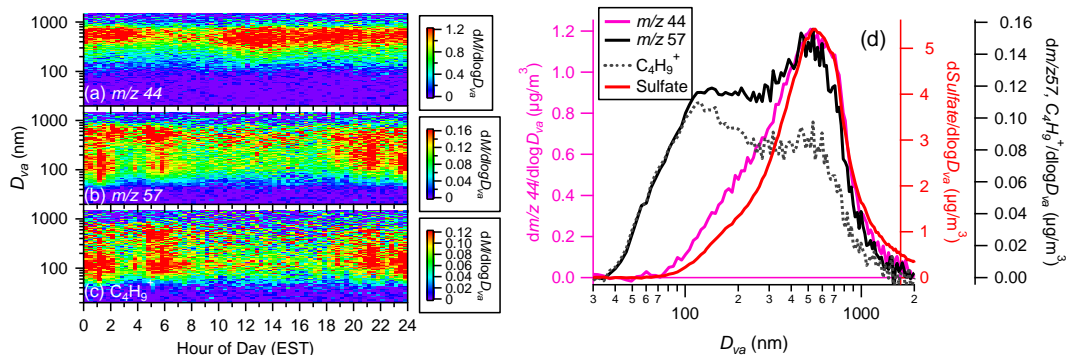
Back | Close

Full Screen / Esc

Printer-friendly Version

Interactive Discussion
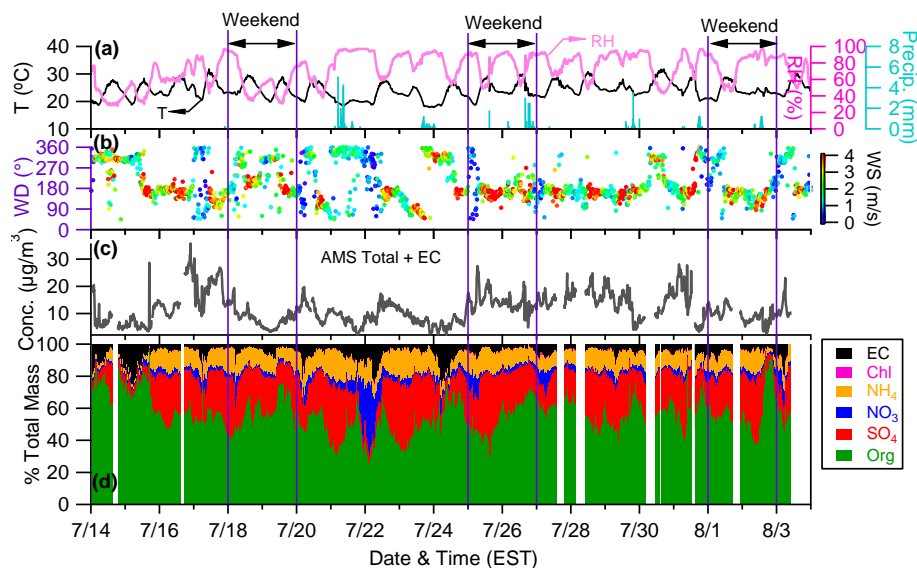
Fig. 2. Time series of **(a)** relative humidity (RH), temperature (T), and hourly precipitation (Precip), **(b)** wind direction (WD) colored by wind speed (WS), **(c)** mass concentration of AMS total+EC, and **(d)** mass fractions of chemical species in PM_1.

Fig. 3. Diurnal profiles of the mass concentrations (solid black circles) and the size distributions of EC, organics, sulfate, nitrate, ammonium, and chloride.

Title Page

Abstract | Introduction

Conclusions | References

Tables | Figures

|◄ | ►|

◄ | ►

Back | Close

Full Screen / Esc

Printer-friendly Version

Interactive Discussion

Fig. 4. Diurnal cycles of **(a)** sulfate, estimated gas phase production rate of H_2SO_4, and CO_2 and **(b)** nitrate, estimated gas phase production rate of HNO_3, equilibrium constant of K_p for ammonium nitrate, and CO_2.

Title Page

Abstract | Introduction

Conclusions | References

Tables | Figures

|◄ | ►|

◄ | ►

Back | Close

Full Screen / Esc

Printer-friendly Version

Interactive Discussion
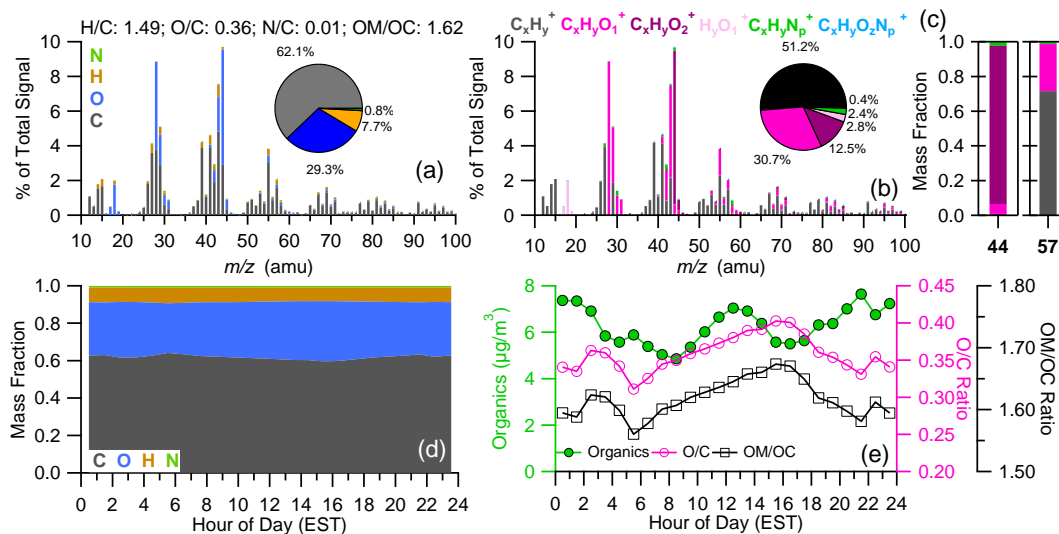
Fig. 5. Average OA spectrum colored by the contributions of **(a)** elements (C, O, H, and N) and **(b)** six ion categories. **(c)** The ion compositions of *m/z* 44 and 57; **(d)** diurnal profile of the mass fractions of elements; and **(e)** diurnal profiles of organics, O/C and OM/OC ratios. The inset pie charts in (a) and (b) show the average mass fractions of elements and ion categories, respectively. The average elemental and OM/OC ratios of OA are also shown in the legend of (a).
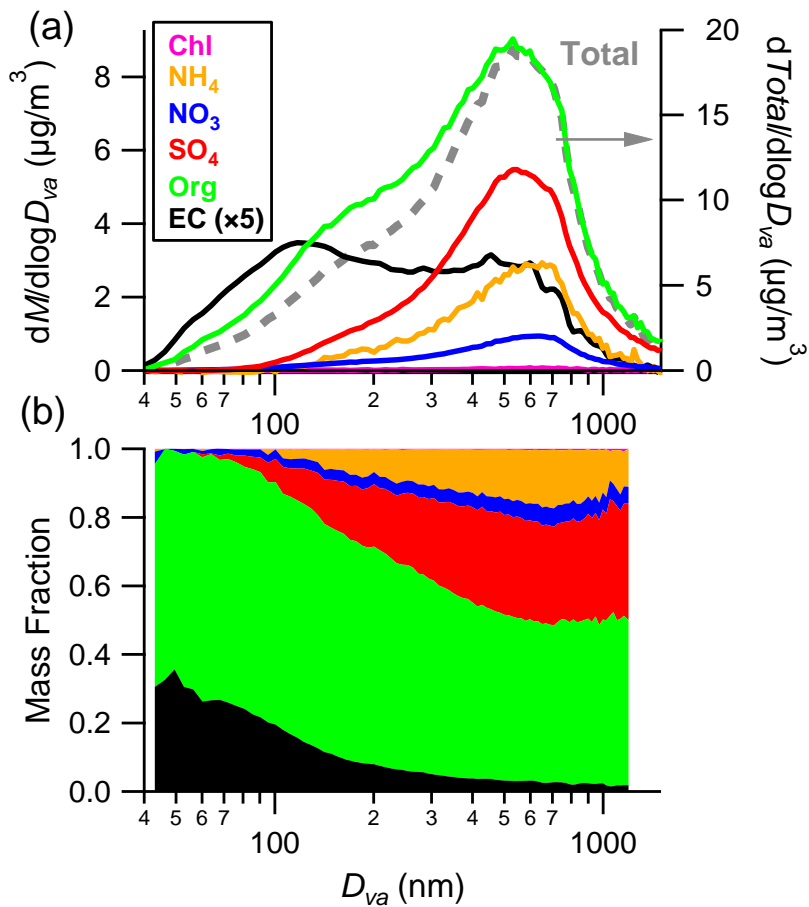
Fig. 6. Average size distributions of **(a)** mass concentrations and **(b)** fractional compositions of submicron aerosol species for the entire study.

Fig. 7. Diurnal evolution of the size distributions of **(a)** m/z 44, **(b)** m/z 57, and **(c)** $C_4H_9^+$. **(d)** The average size distributions of m/z 57, m/z 44, $C_4H_9^+$, and sulfate of the entire study.
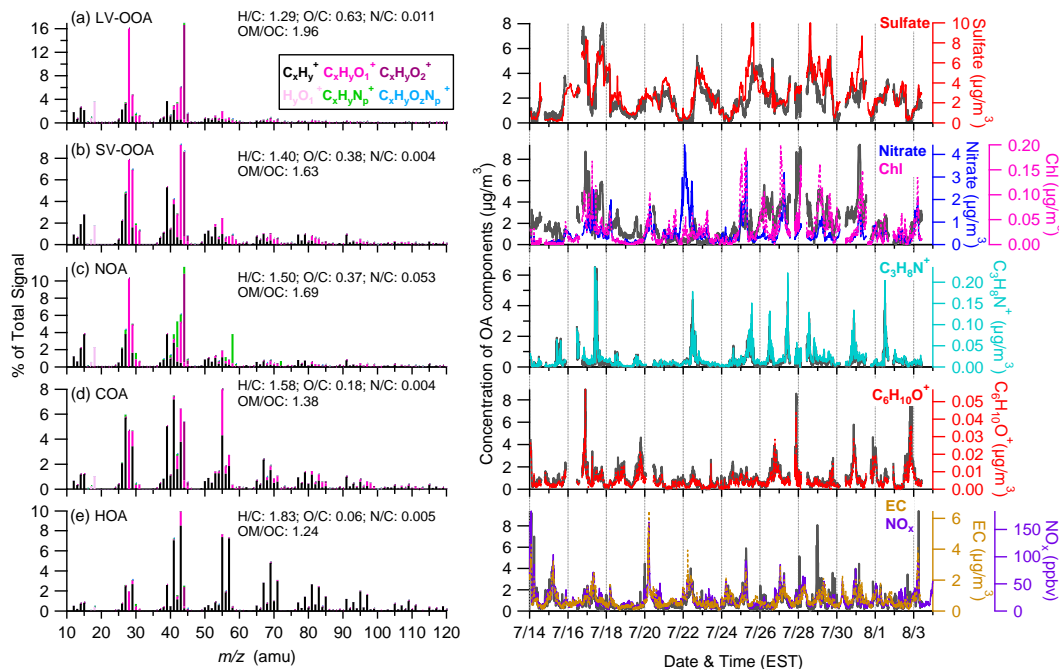
Fig. 8. HRMS (left) and time series (right) of OA components: **(a)** low-volatility oxygenated OA (LV-OOA) **(b)** semi-volatile OOA (SV-OOA), **(c)** nitrogen-enriched OA (NOA), **(d)** cooking-emission OA (COA), and **(e)** hydrocarbon-like OA (HOA). Also shown are the corresponding time trends of tracer compounds, i.e., sulfate for regional secondary species in (a), nitrate and chloride for semi-volatile secondary species in (b), $C_3H_8N^+$ as a tracer ion for amine-type of compounds in (c), $C_6H_{10}O^+$ as a tracer ion for cooking aerosols in (d), and EC and NO_x as tracers for combustion emissions in (e). The elemental ratios and OM/OC ratio of each component are also shown in the legends.

Title Page

Abstract | Introduction

Conclusions | References

Tables | Figures

◄◄ | ►►

◄ | ►

Back | Close

Full Screen / Esc

Printer-friendly Version

Interactive Discussion
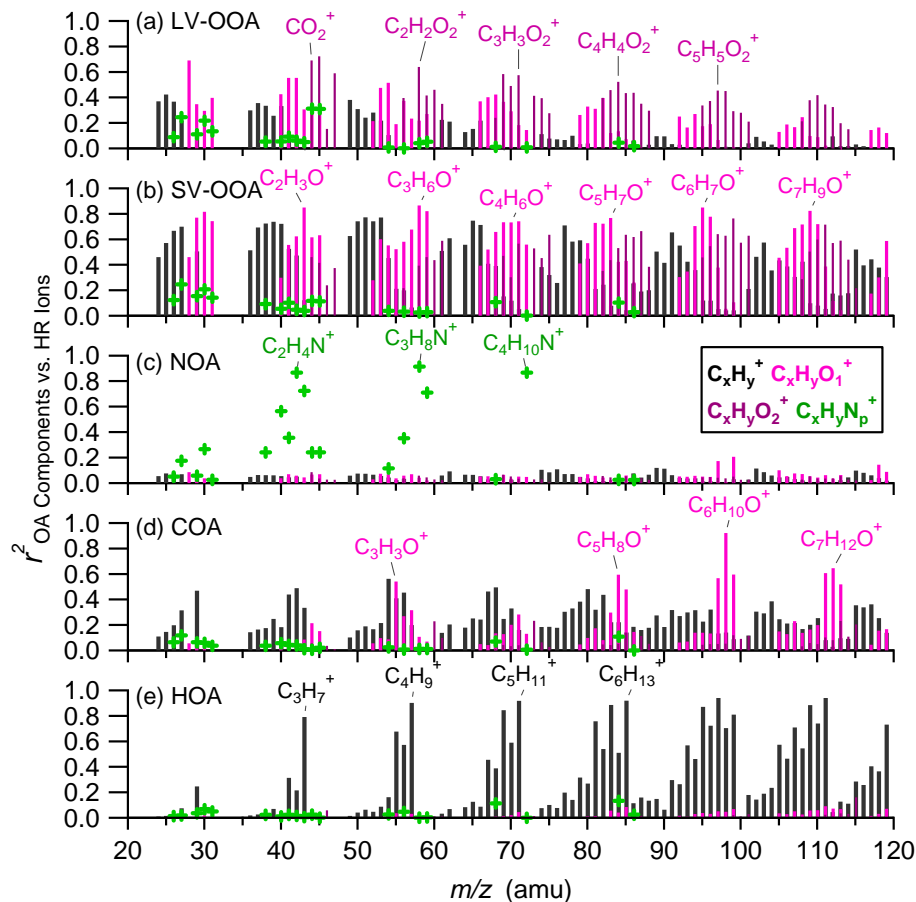
Fig. 9. Correlations of each OA component with the HRMS ions colored by four ion categories, i.e., $C_xH_y^+$, $C_xH_yO_1^+$, $C_xH_yO_2^+$, and $C_xH_yN_p^+$. The formulas of the ions that show significant correlations with individual OA components are marked.
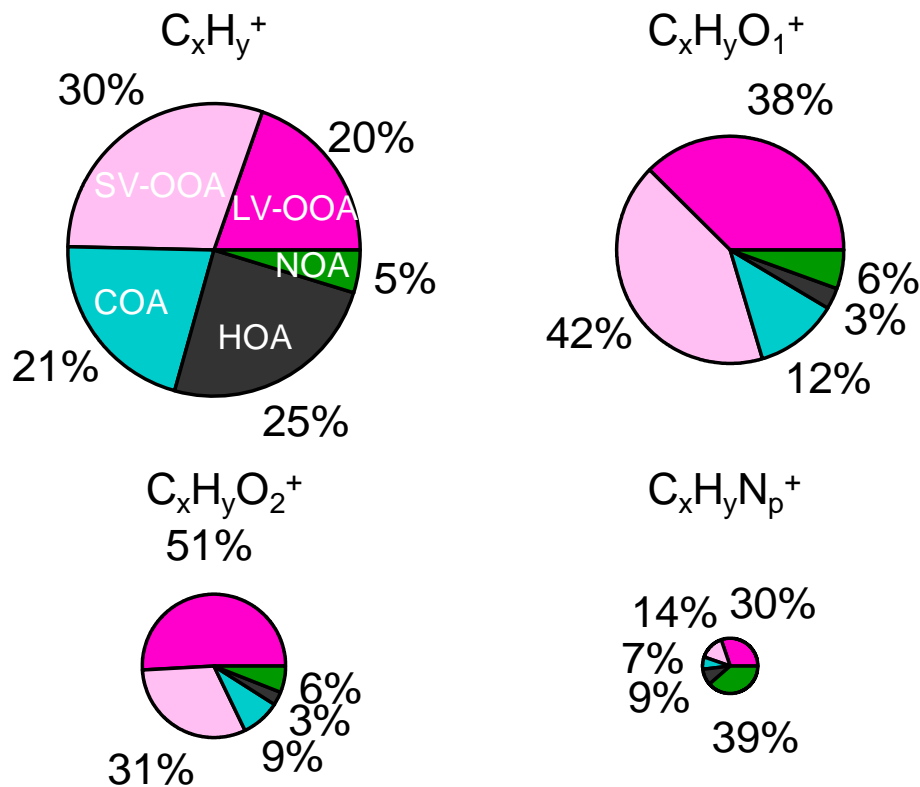
Fig. 10. Average contribution of OA components to four ions categories, i.e., $C_xH_y^+$, $C_xH_yO_1^+$, $C_xH_yO_2^+$, and $C_xH_yN_p^+$, for the entire study. The area of each pie is scaled to be proportional to the mass concentration of the corresponding category.
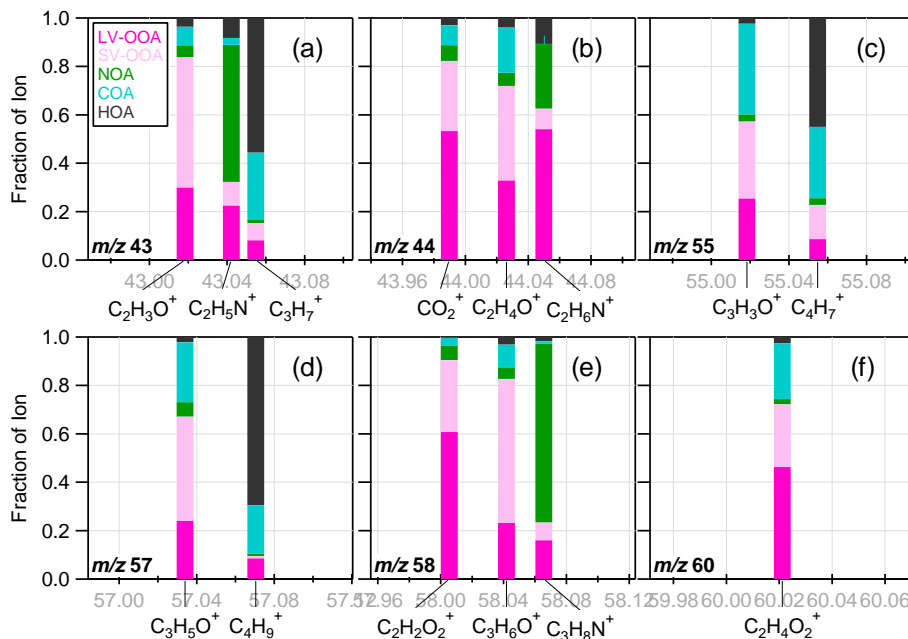
Fig. 11. Average contribution of each OA component to the ions at *m/z* **(a)** 43, **(b)** 44, **(c)** 55, **(d)** 57, **(e)** 58, and **(f)** 60. Note that only the major ions at each *m/z* are shown.

Title Page

Abstract | Introduction

Conclusions | References

Tables | Figures

◄ | ►

◄ | ►

Back | Close

Full Screen / Esc

Printer-friendly Version

Interactive Discussion
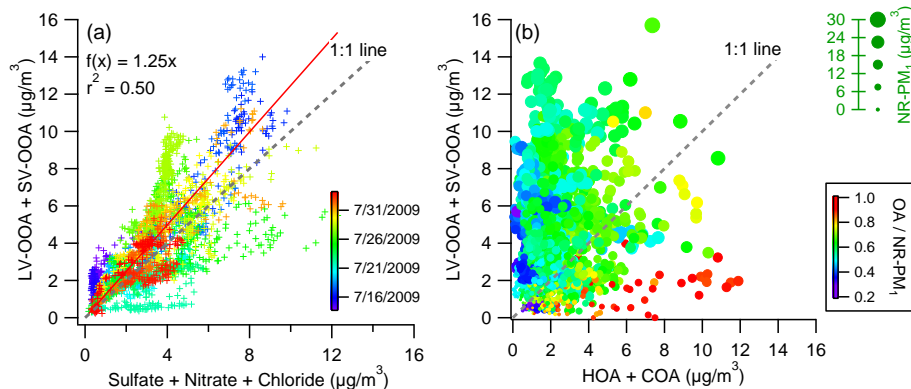
Fig. 12. Correlations of **(a)** total OOA (=LV-OOA+SV-OOA) vs. total secondary inorganic anions (=Sulfate+Nitrate+Chloride). The data fitting was performed using the orthogonal distance regression (ODR), and **(b)** total OOA vs. POA (=HOA+COA), colored by the mass fraction of OA in NR-PM$_1$. The marker size is proportional to the concentration of total NR-PM$_1$.
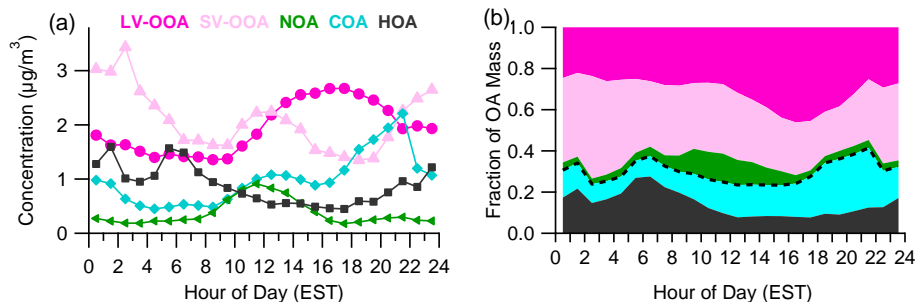
Fig. 13. Diurnal cycles of **(a)** mass concentrations and **(b)** mass fractions of five OA components. The dash line in (b) shows the mass fraction of POA (HOA+COA).
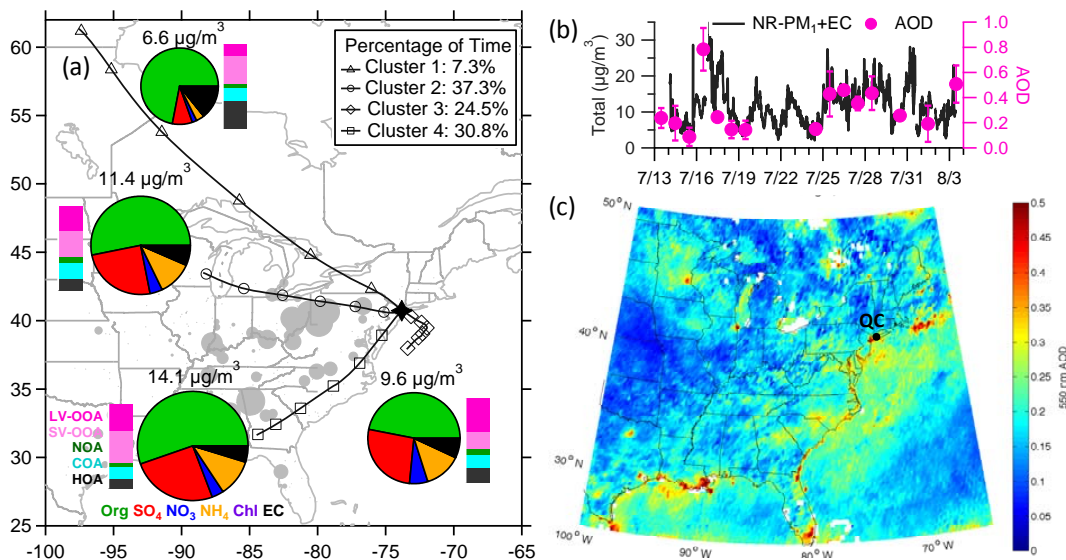
ACPD

10, 22669–22723, 2010

Characterization of organic and inorganic aerosols in New York City

Y.-L. Sun et al.

Title Page

| Abstract | Introduction |

| Conclusions | References |

| Tables | Figures |

|◄ | ►|

◄ | ►

Back | Close

Full Screen / Esc

Printer-friendly Version

Interactive Discussion
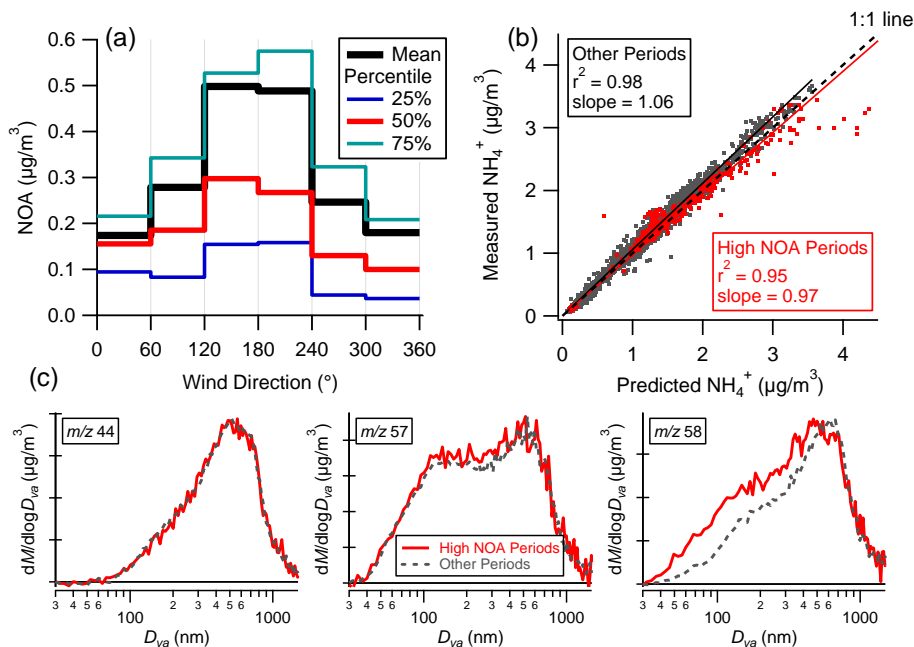
Fig. 14. **(a)** Statistical distributions of NOA concentrations corresponding to different wind sectors, **(b)** correlations between measured NH_4^+ and predicted NH_4^+ (=SO_4^{2-}/96×36+NO_3^-/62×18+Cl^-/35.5×18; Zhang et al., 2007b), and **(c)** average size distributions of m/z 44, 57, and 58 during high NOA periods vs. the rest of the times, respectively. The size distributions in (c) are all scaled to their corresponding maxima for better comparisons of peak shapes.

Fig. 15. (a) Average composition of PM_1 (pie charts) and OA (bar charts) for each cluster. The markers on the trajectories indicate 12 h interval. The area of the pie chart is proportional to the total mass of PM_1. The solid grey circles show the distribution of SO_2 emission sources from the EPA's National Emission Inventory database (http://www.epa.gov/air/data/netemis.html). Bigger size indicates larger emissions. **(b)** Time series of total mass of PM_1 and AOD retrieved from Terra MODIS at 550 nm and **(c)** distribution of average AOD for the entire study.